Solar Probe: First Mission to the Nearest Star

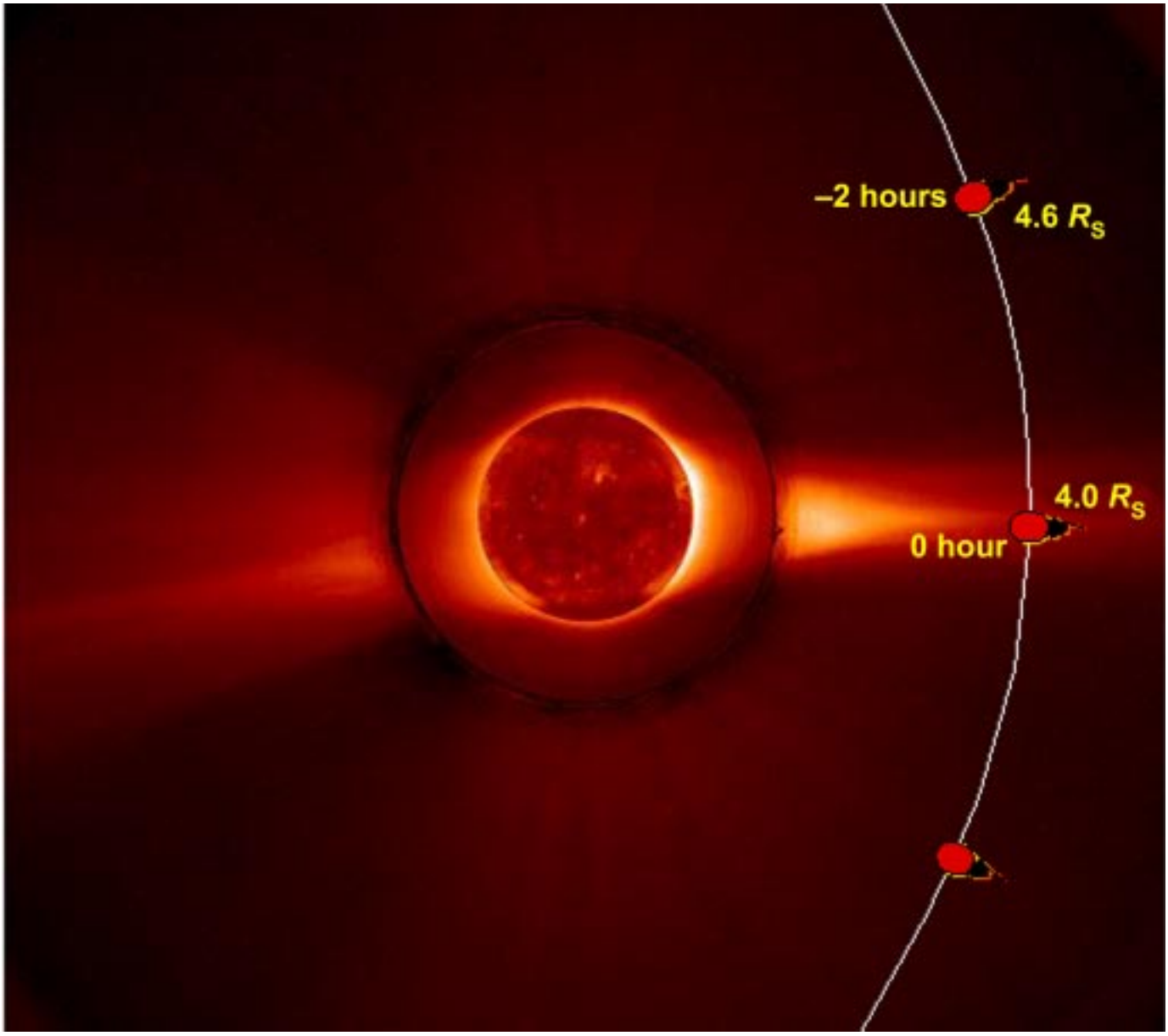

Report of the NASA Science Definition Team for the Solar Probe Mission

Solar Probe: First Mission to the Nearest Star

Report of the NASA Science Definition Team for the Solar Probe Mission

Edited and published at The Johns Hopkins University Applied Physics Laboratory, Laurel, Maryland, February 1999.

Solar Probe Science Definition Team

Chairman
George Gloeckler
Dept. of Physics and Astronomy
University of Maryland
College Park, Maryland

Members
William C. Feldman
Los Alamos National Laboratories
Los Alamos, New Mexico

Shadia R. Habbal
Harvard Smithsonian Center for Astrophysics
Cambridge, Massachusetts

Clarence M. Korendyke
Naval Research Laboratory
Washington, D.C.

Paulett C. Liewer
NASA/Jet Propulsion Laboratory
Pasadena, California

Deputy Chair
Ralph L. McNutt, Jr.
The Johns Hopkins University
Applied Physics Laboratory
Laurel, MD

Eberhard Möbius
Space Science Center
University of New Hampshire
Durham, New Hampshire

Thomas E. Moore
NASA/ Goddard Space Flight Center
Greenbelt, Maryland

Stewart L. Moses
TRW Space and Technology Group
Redondo Beach, California

Study Manager
James E. Randolph
NASA/Jet Propulsion Laboratory
Pasadena, California

Robert Rosner
Astronomy and Physics, Fermi Institute
University of Chicago
Chicago, Illinois

James A. Slavin
NASA/Goddard Space Flight Center
Greenbelt, Maryland

Steven T. Suess
NASA/Marshall Space Flight Center
Huntsville, Alabama

Alan M. Title
Martin-Lockheed Research
Palo Alto, California

Project Scientist
Bruce T. Tsurutani
NASA/Jet Propulsion Laboratory
Pasadena, California

Acknowledgments

The Solar Probe Science Definition Team would like to thank Karla Clark, Kenneth Klaasen, and Bruce Goldstein of JPL for their valuable technical assistance; John Arballo of JPL for his help with the artwork; and Margaret Morris of JHU/APL for editorial work in the preparation of this report. Publication of this report was supported by NASA grant NAG5-6113. We are especially grateful to James Ling of NASA Headquarters for his sensible advice and constant encouragement. The technical work for this mission was supported by the JPL Study Team, consisting of J. A. Ayon (Mission Analysis and Systems Engineering), B. E. Goldstein (Science), S. Eremenko (Configuration), E. Mettler (Attitude Control), R. N. Miyake (Thermal), W. V. Moore (Telecommunication), W. Imbriale (Antenna), B. J. Nesmith (Power), and J. E. Randolph (Study Manager). Finally, we also acknowledge important contributions from past Solar Probe Science Definition Teams, as well as the interest and support for the Solar Probe Mission from many members of the scientific community.

Table of Contents

Executive Summary

The solar corona is one of the last unexplored regions of the solar system and one of the most important regions for understanding Sun–Earth Connections. Results from the Solar Orbiting Heliospheric Observatory (SOHO) and Ulysses have focused understanding of regions to the point that *in situ* measurements and close-up imaging are necessary for further progress.

This report describes a robust, scientifically important space mission to explore the source of the solar wind from inside the solar corona at 4 to 110 solar radii from the center of the Sun.

Our primary science objective is to understand the processes that heat the solar corona and produce the solar wind. Solar Probe, the third of three missions in NASA's Outer Solar System/Solar Probe Project, will accomplish this objective with a combination of *in situ* particle and fields measurements and remote sensing. The *in situ* instruments will measure structures of various scales, including some of the smallest filamentary structures, transients, and waves in coronal holes and streamers; the remote sensing instruments will detect both small-scale, transient magnetic structures and global coronal conditions at the Sun. Payload development is streamlined by having each of the two classes of instruments built under the direction of a single principal investigator (that is, all sensors under one PI):

- ***In situ* measurements:** plasma distribution functions and composition; plasma waves; energetic particle fluxes and composition; magnetic fields
- **Remote sensing:** magnetograph/Doppler (helioseismology) imaging of the Sun; high-spatial-resolution extreme ultraviolet/X-ray imaging of the Sun; coronal imaging

The mission and spacecraft designs were derived from concepts developed during earlier mission studies, but important differences reduce cost and enhance science return:

- The focused science objectives are met with a science payload mass of up to 19 kilograms that requires no more than 16 watts and delivers a data return greater than 100 kilobits per second.
- The vehicle design incorporates nadir viewing capability for both imaging and particle sensing.

The trajectory lies in the plane perpendicular to the ecliptic. Perihelion distance is 4 solar radii from the center of the Sun following a Jupiter gravity assist. The mission consists of two near-Sun flybys. With a 2007 launch, the first pass occurs near solar maximum. The second pass occurs in the descending phase of the solar cycle, near solar minimum.

1. Overview

Solar Probe, the first mission to the Sun and the third of three missions in NASA's Outer Solar System/ Solar Probe Project, is a voyage of exploration, discovery, and comprehension. For decades, space scientists have anticipated this mission to the inner frontier of the heliosphere. This near-Sun flyby will provide *in situ* measurements in the solar corona and high-resolution pictures and magnetograms of the photosphere and polar atmosphere. By flying through coronal holes, where fast solar wind is believed to be born, and through streamers, where slow solar wind most likely originates, and by determining solar surface properties over the poles, Solar Probe addresses the basic questions of solar wind origin. Such measurements can be obtained in no other way, yet they are absolutely necessary, both to unravel this mystery of the solar wind and to explain what fundamental natural processes require the Sun (and probably most other stars) to have a million-degree corona. These measurements also are needed as "ground truth" for interpreting the many measurements of the Sun and solar activity that have been made from a distance of 1 AU. Driven by the extraordinary observations from Ulysses and the Solar Orbiting Heliospheric Observatory (SOHO), Solar Probe measurements made close to the Sun can provide closure to these fundamental problems.

Solar Probe is scheduled for launch in February 2007. It will arrive at the Sun along a polar trajectory perpendicular to the Sun–Earth line with a perihelion of 4 solar radii (R_S) from the Sun's center. Two perihelion passages will occur, the first in 2010 (near solar sunspot maximum) and the second in 2015 (near solar minimum), ensuring measurement of both coronal hole and streamer-related solar wind properties. To reach the Sun, the probe must first fly to Jupiter and use a gravity assist to lose its angular momentum about the Sun. The Jupiter flyby also rotates the probe's orbital plane 90° away from the ecliptic. Dropping into the Sun some 3.6 years after launch, Solar Probe passes 0.5 AU 10 days prior to closest approach and spends an intense ~14 hours between the north and south solar poles. The imaging and *in situ* miniaturized instruments will provide the first 3-dimensional view of the corona, high spatial- and temporal-resolution observations of the magnetic fields, and helioseismic measurements of the polar regions, as well as local sampling (at times at high spatial resolution) of plasmas and fields at all latitudes. The first encounter is timed to provide passage over the west limb of the Sun to enable a real-time data link during the flyby. During the same solar rotation but before the flyby, this geometry allows Earth-based observers to preview the longitude traversed by Solar Probe at perihelion. Scientific discussions of various aspects of the Solar Probe mission have been reported recently in the literature (Habbal, 1997; Möbius et al., 1999; Gloeckler et al., 1999b; Habbal et al., 1998).

1.1 The Need

One of the last unexplored regions of the solar system is the innermost portion of the heliosphere: the region inside the orbit of Mercury. We have flown by many planets. Galileo is now orbiting Jupiter, and Cassini is on its way to Saturn. With Ulysses we are exploring the high-latitude heliosphere. The Voyagers will soon reach and report on the distant boundary of the solar system. From its 1-AU orbit, SOHO is imaging the Sun and its atmosphere far better than ever before. Wind and ACE are measuring solar wind and solar energetic particles at 1 AU with unsurpassed precision and detail. Yet we have never encountered the Sun. The inner heliosphere, the solar corona, and polar photosphere remain essentially unexplored. At the same time, Ulysses and SOHO have shown us that we do not understand how energy flows into the solar atmosphere, heats the corona and drives the solar wind, which affects the Earth and all other planets and determines the size and shape of the heliosphere. It is now clear that only *in situ* measurements offer the opportunity to achieve that understanding.

It is now technically possible to send a well-instrumented and affordable spacecraft close to the Sun's surface to explore for the first time this last frontier—the inner heliosphere from a few solar radii to ~60 R_S. Solar Probe is this mission.

Flying from pole to pole of the Sun through the solar atmosphere down to 4 R_S from the Sun's center, Solar Probe will perform the first close-up exploration of the Sun, the only star accessible to humankind. This pioneering mission will directly sample the solar wind in the acceleration region and will take high-resolution images of the solar atmosphere and

of the polar regions of the Sun's surface. This missing "ground truth" picture will link the enormous wealth of existing solar and coronal observations to the actual physical state and dynamics of the solar corona. Solar Probe will take us a long way toward determining the origin and acceleration of the fast and the slow solar wind that engulfs the entire solar system, modulates the penetrating cosmic rays from the galaxy into the solar system and onto Earth, and controls interplanetary space from the Sun to the local interstellar medium far beyond the outermost planets.

1.2 Current Knowledge of the Solar Wind

Fast and Slow Solar Wind. Ulysses, with its near-polar 1.4 × 5.4 AU orbit, revealed that solar wind comes in two states: an irregular slow wind with typical speeds of 400 km/s and a smooth fast wind with a speed of ~750 km/s. This "bimodality" of the solar wind is most apparent at solar minimum. Fast wind comes from coronal holes, and slow wind comes from the boundaries or interior of streamers. Solar Probe will encounter streamers in both 2010 and 2015 and will pass through coronal holes at 5 to 10 R_S in 2015.

Fast Wind is Steady and Simple. Fast wind is relatively steady and also relatively simple in composition. Its charge-state distribution is characterized by a single, low freezing-in coronal temperature for each element. The elemental composition of the solar wind is less biased in the fast wind than tends to be the case in the slow wind; it resembles the photospheric composition more closely than is generally true with the slow wind; and the overabundance of low first ionization potential (FIP) elements is much weaker in the fast wind than it is in the slow wind. Fast wind is permeated by an evolving field of magnetohydrodynamic (MHD) turbulence, which is presumed to be a remnant or imprint of the coronal acceleration process.

Slow Wind is Variable and Complicated. Slow wind is highly variable in speed and more complicated than fast wind in its other characteristics. Its charge-state distribution can no longer be characterized by a single freezing-in temperature. The FIP effect is far more pronounced, and the ^{3}He/^{4}He ratio is both higher and more variable in the slow wind than in the fast wind. MHD turbulence in slow wind is less evolved and more intermittent than in fast wind.

The Boundary Between Fast and Slow Wind is Sharp. This boundary between fast and slow wind is also sharp in freezing-in temperature and FIP strength. Thus the boundary between fast and slow wind must extend down to the lower corona, where the charge states freeze in, and to the chromosphere, where the composition is established.

1.3 Current Knowledge of the Corona and High-Latitude Solar Photosphere

Coronal Structure and the Solar Cycle. The corona changes dramatically over the solar cycle, with coronal holes dominating at sunspot minimum and essentially absent at solar maximum. Streamers dominate the corona outside of coronal holes. Solar Probe will pass through the corona at both solar maximum and solar minimum to provide good data on both steamers and coronal holes.

Characteristics of the Initial Solar Wind in Coronal Holes. SOHO and interplanetary scintillation results show that fast wind reaches its terminal speed by 10 R_S and that at 4 R_S it is already being accelerated. At 4 R_S the temperature of heavy ions is much higher than that of protons, whereas at 1 AU, the difference is smaller. The proton temperature at 4 R_S in coronal holes is 2 to 3 times higher than the electron temperature inferred from charge state measurements in the terminal wind, but they differ by less than a factor of 2 at 1 AU. Inferred ion temperature anisotropies are enormous between 2 and 10 R_S and are believed due to an Alfvén or ion-cyclotron wave field absorption contributing to the perpendicular temperature. A true proton temperature anisotropy exists in the 1-AU fast solar wind, but it is smaller than inferred from the coronal observations.

Plumes permeate all coronal holes, yet are invisible in the solar wind. How this variable, filamented flow becomes the uniform fast wind is unknown. Solar Probe will answer the question of whether this transition is related to the source and evolution of wave turbulence in the solar wind.

Characteristics of the Initial Solar Wind in and Above Streamers. Results from SOHO and other observations indicate that flow speeds in and around streamers are consistent with the origin of slow wind, but how this happens has not been determined. One problem is that the standard concept of a streamer is a magnetostatic structure that releases no wind in the steady state. However, SOHO has clearly shown sporadic escapes of mass from the tops of streamers that seem to ride on a preexisting subsonic slow flow. Solar Probe will pass through the tops of streamers precisely where this process is occurring.

Measurements from SOHO show that the proton temperature is comparable to or lower than the inferred electron temperature, but proton temperature is distinctly less than electron temperature in the terminal solar wind. Inferred ion temperature anisotropies are less than in coronal holes. Composition measurements in streamers show a difference in core and boundary composition that is consistent with an essentially static core. Solar Probe will measure how these differences map out into the solar wind.

Properties of the Polar Photosphere. SOHO has hinted at some remarkable features for the polar photosphere. But since neither SOHO nor any spacecraft confined to near the ecliptic plane can view the poles effectively, these features remain poorly defined. The SOHO results show

1. A rotation rate at higher latitudes that is even lower by 10% to 20% than expected from extrapolation of mid-latitude differential rotation
2. Some evidence for a polar vortex
3. Some evidence of a polar concentration of magnetic flux
4. Measurements of surface and subsurface motion indicating that meridional flows are a factor of more than 2 higher than previously estimated
5. Indications that small- and large-scale magnetic fields on the Sun are rooted at different depths in the convection zone

Combined with the more general SOHO result showing that magnetic flux is replaced very rapidly everywhere on the surface of the Sun (approximately every 40 hours), these results suggest the value of a close examination of the photospheric dynamics and magnetic fields. Such a close examination will extend our understanding of how those dynamics and fields relate to the flow of energy into the corona.

1.4 Summary

The results briefly described in Sections 1.2 and 1.3 leave many fundamental questions unresolved about the solar wind origin and the mechanisms for its acceleration, as well as about coronal heating mechanisms and flow of energy from the solar surface to the corona. We do not know magnetic field phenomenology and surface and subsurface flow patterns in the polar regions and how they differ from those at lower latitudes. We have no direct information on the nature of wave turbulence and of wave–plasma interactions in the acceleration region. We have no direct information on the energetic particle populations, their production and acceleration. Turbulence in the upper corona and transient events at lower altitudes provide appropriate conditions for particle acceleration. Identification of the active mechanisms will depend on knowing the underlying particle population and wave environments, along with their spatial extent and dynamical evolution.

All of these questions will remain unanswered until *in situ* measurements are made in the solar wind acceleration region near the Sun and until high-resolution images of the polar regions of the Sun are taken. These questions are the basis for the Solar Probe Mission.

2. Current Scientific Understanding and Questions

2.1 The Sun, the Corona, and the Solar Probe Mission

Solar Probe will fly as close to the Sun's surface as is possible with today's technology. Both imaging and *in situ* measurements will provide the first 3-dimensional view of the corona, high spatial- and temporal-resolution measurements of the plasma and magnetic fields, and high-resolution helioseismology and magnetic field observations of the solar polar photosphere. Two perihelion passes are planned, the first near the 2010 sunspot maximum and the second near the 2015 sunspot minimum, when the solar corona will be similar to that shown in the image on

the cover of this report. At its perihelion of 4 R_S, Solar Probe will be immersed in bright equatorial streamers like those on the cover. In this region, the plasma is dense and dominated by collisions; the plasma ratio of thermal pressure to magnetic pressure $\beta > 1$; the speed is subsonic; and slow solar wind originates in a way that has so far eluded understanding. Elsewhere, at 5 to 20 R_S, Solar Probe will pass through coronal holes where the fast solar wind originates. Here, the plasma is collisionless and non-Maxwellian, and the plasma $\beta << 1$.

The primary unanswered questions:

Solar Probe will address the following unanswered questions about basic physical phenomena of the Sun:

- What is the physics of the flow of energy through the Sun's surface and into the solar atmosphere (corona)?
- What causes the slow solar wind? What causes the fast solar wind?
- What are the properties of the smallest structures in coronal holes and streamers?
- What are the magnetic fields and solar rotation like near the poles of the Sun, beneath the polar coronal holes?

There are several alternative scenarios for what this mission may reveal, and each scenario is related to specific causes for coronal expansion. Solar Probe's ensemble of instruments will provide the specific information needed to distinguish between these scenarios, fulfilling the mission's overall objective. The mission will furthermore link the enormous wealth of existing solar and coronal observations to the actual physical state and dynamics of the solar corona. This pioneering mission meets basic needs of the NASA Solar Connections Initiatives. It is of fundamental significance in astrophysics, because the Sun is the prototype for all other stars and is the only star that can be investigated in detail.

Solar Probe makes two full orbits about the Sun to allow observations in the corona near both solar maximum and solar minimum. This requirement comes from the radically changing nature of the corona over the 11-year solar sunspot cycle and the "bimodality" of the solar wind. The solar cycle changes in the corona are shown schematically in Figure 1.

Near solar maximum, the large-scale magnetic field of the Sun is disordered, coronal mass ejections (CMEs) occur at a rate of several per day, many solar flares occur each day, and radio, extreme ultraviolet (EUV), and X-ray emissions from the corona are orders of magnitude higher than at solar minimum. Long-lived coronal holes are either absent or very small, Solar Probe has a negligible probability of encountering one. During this time (Figure 1a), Solar Probe will collect information on the active Sun and corona, on the source of the slow wind, on shock waves and plasma waves, and on the acceleration of energetic particles in the corona.

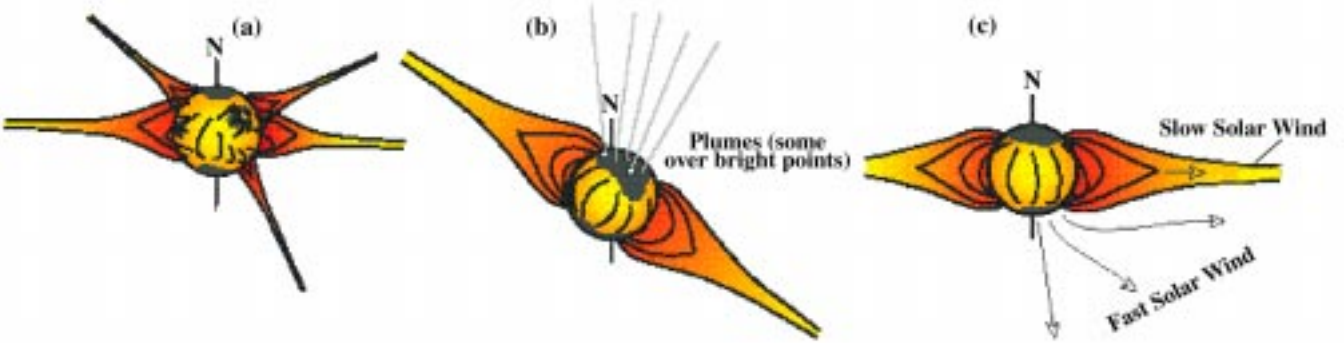

Figure 1. Schematic of evolution of the solar corona over the 11-year sunspot cycle. (a) Solar maximum, when the Sun is covered by relatively small streamers with small or nonexistent polar coronal holes. (b) Declining phase of the solar cycle, also showing that coronal plumes occur in the coronal holes. Plumes, however, exist at all times in coronal holes. The polar coronal holes are growing in size at this time and the global structure of the corona often appears "tilted" away from the rotation axis (N). (c) Solar minimum, similar to the configuration seen in the image on the cover of this report. At minimum, the polar coronal holes are at their largest.

Near solar minimum, the Sun's global magnetic field is well organized and roughly dipolar. The corona is dominated by large equatorial streamers, and polar coronal holes extend down to mid-latitudes at the photosphere and nearly to the equator beyond a few solar radii (Figure 1c). CMEs occur at a rate of about one per day. During this time, Solar Probe is certain to pass through a polar coronal hole inside 8 R_S, and probably inside 5 R_S. Detailed measurements of the properties of fine structure, waves, and turbulence in the high-speed wind will be made, and the properties of quiescent equatorial streamers can be determined. This phase of the mission will resolve the many questions about the origin of fast solar wind.

Objectives of the Solar Probe mission:

The irreductable core objectives (category A; see Section 3.1) of the Solar Probe mission, defined from the unanswered questions just listed and from known properties of the corona, are as follows:

- Determine the acceleration processes and find the source regions of fast and slow solar wind at maximum and minimum solar activity.
- Locate the sources and trace the flow of energy that heats the corona.
- Construct the 3-dimensional coronal density configuration from pole to pole and determine the subsurface flow pattern, the structure of the polar magnetic field, and its relationship with the overlying corona.
- Identify the acceleration mechanisms and locate the source regions of energetic particles, both to understand the physical processes responsible and to use the particles to probe, remotely, physical conditions in the plasma; determine the role of plasma waves and turbulence in the production of solar wind and energetic particles.

Because the properties of the corona are so dependent on the solar cycle, these mission objectives cannot be met in a single pass of the Sun at any single time during the solar cycle. However, the use of two passes through the corona at appropriately different times in the solar cycle allows the mission to meet all objectives.

The following sections give details on what is known of the solar corona and why Solar Probe is necessary to address the unanswered questions.

2.2 Results from Ulysses that Motivate the Solar Probe Mission

A major result from Ulysses is a graphic picture of solar wind bimodality—meaning that the slow solar wind and the fast solar wind have fundamentally different origins. Evidence for bimodality is outlined in Table 1.

The graphic picture of bimodality is the "dial plot" (Figure 2) of solar wind speed versus heliographic latitude measured by Ulysses between 1994 and 1995 during the fast latitude scan from 80°S to 80°N latitude. (Ulysses was ~2.2 AU over the poles and ~1.4 AU at perihelion, at the equator.) This plot shows that fast wind is steady and that the transition to slow wind is nearly discontinuous, occurring here

Table 1. Bimodality of the solar wind.

Property (1 AU)	Slow Wind	Fast Wind
Flow speed	400 km/s Variance ~50%	750 km/s Variance ~5%
Density	7 cm^{-3} Variance 50–100%	3 cm^{-3} Variance 10–30%
Temperature	T_p(1 AU) ~ 50,000 K Variance 50–100%	T_p(1 AU) ~ 200,000 K Variance 50–100%
Composition	Depends strongly on first ionization potential (FIP)	Nearly independent of FIP
"Freezing-in" temperature	~1.5×10^6 K	~10^6 K

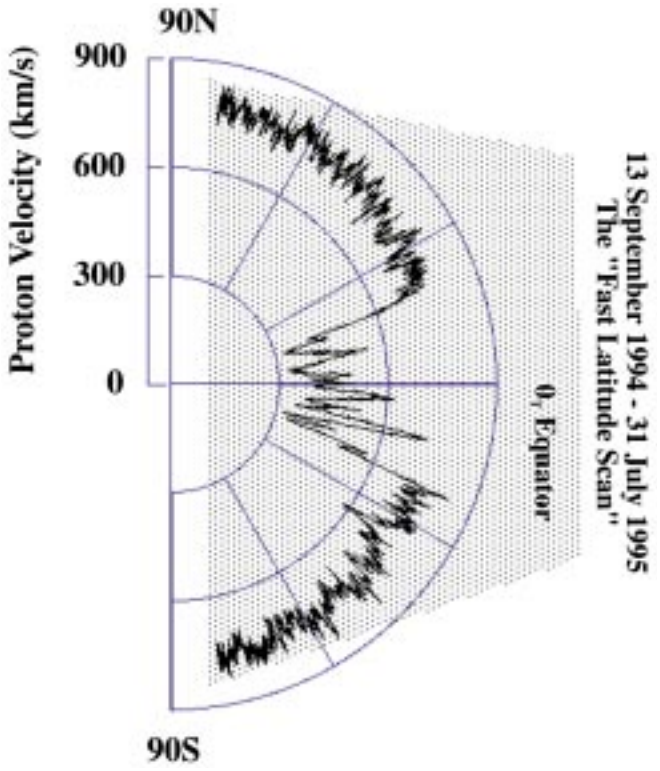

Figure 2. "Dial plot" of flow speed measured with Ulysses during the 1-year fast latitude scan. Variance in the high speed is ~5% over this interval (McComas et al., 1998).

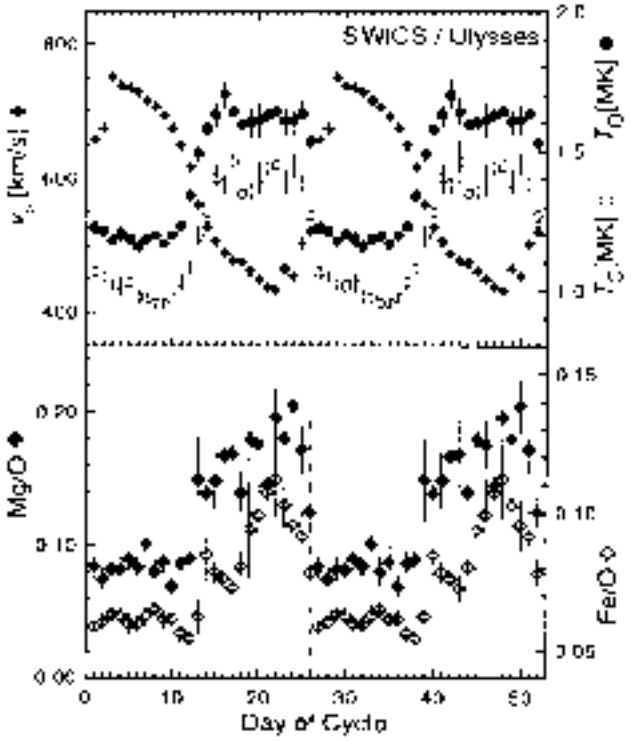

Figure 3. Solar wind He speed (pluses), O (closed circles) and C (open circles) coronal freezing-in temperature, as well as Mg/O (closed diamonds) and Fe/O (open diamonds) abundance ratios. These Ulysses data are repeated to facilitate recognition of the sharp boundary between fast and slow wind (Geiss et al., 1996).

at latitudes of about ±15°. Figure 2 shows the configuration near solar minimum. (It is expected that near solar maximum the region of steady, fast wind will be much smaller or absent). Measurements at high temporal resolution show that fast wind contains a field of evolving MHD turbulence, whereas fluctuations in the slow wind are of longer period and are more characteristic of a transient source than in the fast wind.

Ulysses observations reveal that the composition of fast wind is also relatively simple. The charge-state distributions indicate a low freezing-in temperature, as is shown for O and C in the top panel of Figure 3. Furthermore, the fast wind distributions of various elements are characterized by a single freezing-in temperature for each element that differs, however, from one species to the next. The composition is least biased in the fast wind (closely resembling photospheric composition), as shown by the abundance of Mg and Fe relative to O in the bottom panel of Figure 3. In contrast, Mg and Fe are overabundant, and the freezing-in temperatures are high and variable in slow wind. These close correlations with flow speed for a coronal process (freezing-in temperature) and a chromospheric process (composition) show that the boundary between fast and slow wind is a sharp boundary extending all the way down to the chromosphere. This is one reason for the current belief that slow wind originates in streamers.

The proton kinetic temperature from the fast latitude scan is shown in Figure 4. There is again the sharp transition in temperature, from the consistently high value in the fast wind to the low value in the slow wind between equatorial high-speed streams. However, the variance in fast wind's temperature is ~50%, compared with its flow speed variance of 5%. This 50% variance is a true variance that is difficult to reconcile with the smooth flow speed shown in Figure 2. It may be the consequence of filamentary structures in the corona such as plumes (which are discussed in more detail in Section 2.3) but this cannot be known until Solar Probe makes the necessary *in*

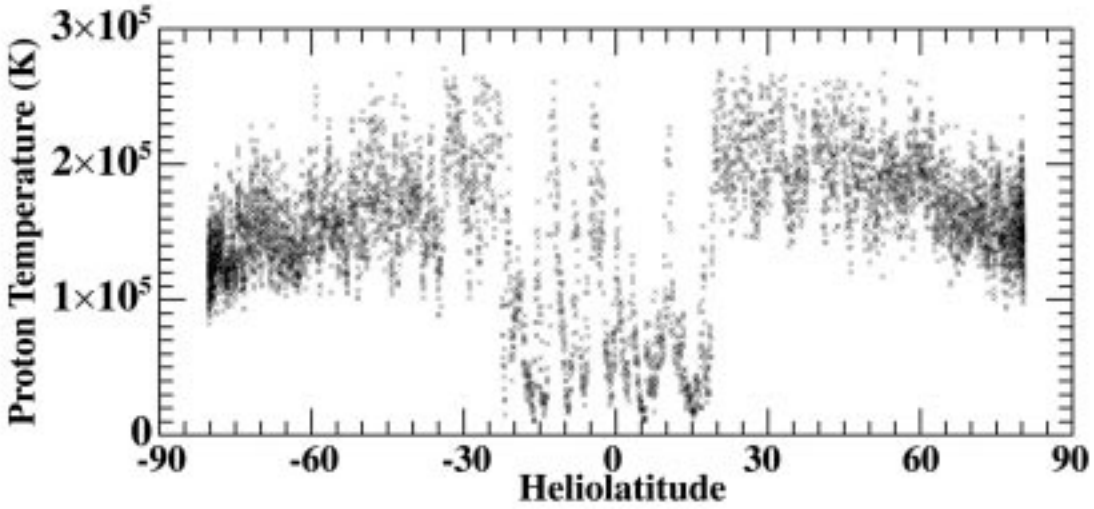

Figure 4. Proton temperatures (1-hour averages, not adjusted for radius) measured during the fast latitude scan from Ulysses.

situ measurements. The kinetic temperature of the slow wind has a comparable variance but differing statistical properties and several large spikes that may result from high-speed equatorial coronal hole flows or from the small CMEs (e.g., Sheeley et al., 1997) that occur even at sunspot minimum. The proton temperature in the fast wind is also anisotropic, being larger perpendicular to the magnetic field than parallel to the magnetic field (Figure 5). This phenomenon is shown in Section 2.3 to have a coronal counterpart in the observations made by SOHO's Ultraviolet Coronagraph Spectrometer (UVCS). Temperature anisotropy is a diagnostic used to distinguish between suspected coronal heating processes because it tests whether high-frequency Alfvén/cyclotron waves may be involved. Solar Probe will measure this parameter as a function of distance all the way into the corona.

What we know as a consequence of Ulysses and other solar wind observations:

- The solar wind is bimodal, and the two states differ in composition, temperature, temperature anisotropy, speed, small-scale fluctuations, and intrinsic variabilities.
- The fundamental importance of these differences was appreciated after only Ulysses' first orbit.

What needs to be answered with Solar Probe:

- How are the differences between the two states created in the solar corona?

2.3 Remote Sensing of the Corona and Photosphere—Fast Wind and the Solar Probe

Ulysses results contrast with what has been learned about streamers and coronal holes with remote

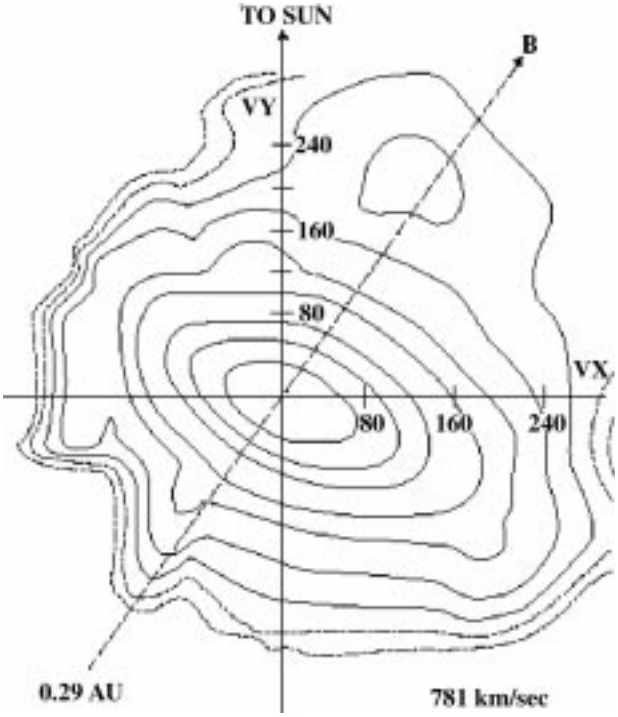

Figure 5. Contours of solar wind proton velocity distribution in fast wind at 0.29 AU measured by Helios. Contours are 0.8, 0.6, 0.4, 0.2, 0.1, 0.03, 0.01, 0.003 and 0.001 of the maximum phase space density. The distribution is anisotropic ($T_{perp} > T_{parallel}$), hot, and has a faster component along the magnetic field direction (dashed line) (Marsch et al., 1982).

sensing from SOHO, as well as results from Interplanetary Scintillations (IPS), Spartan 201-01, and other missions. The comparison raises additional questions. A summary plot of IPS data from the corona, together with some Spartan 201-01 data, is given in Figure 6. The figure shows that the fast wind, on average, already undergoes acceleration inside 4 R_S. Although some acceleration must therefore occur inside Solar Probe's perihelion, the mission will still be able to analyze acceleration physics, as shown in the following paragraph. What is remarkable about Figure 6 is that the vertical spread in individual measurements represents true velocity dispersion. The flow is simply not smooth and well ordered. It appears that at ~5 R_S, flow speeds can be as low as ~400 km/s and as high as 1000 km/s. This dispersion decreases with increasing distance until it converges on the speed observed at Ulysses. This observation has suggested at least three interpretations: (1) the flow is highly filamentary and becomes mixed beyond ~10 R_S; (2) the speed along a streamline is highly variable in time and smoothes dynamically with increasing distance; and (3) the dispersion represents a field of large-amplitude Alfvén waves superimposed on the flow.

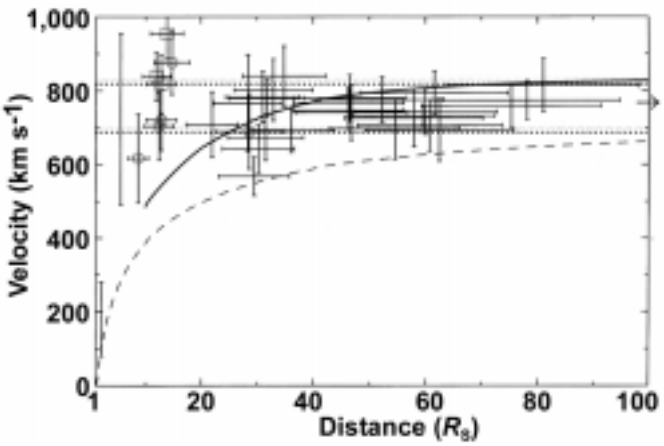

Figure 6. Solar wind speed in coronal holes versus radius with 90% confidence limits (Grall et al, 1996). Also shown are Spartan 201-01 speeds at 2 and 5.5 R_S. The curves are model solutions (dashed) and models plus wave bias (solid). It is concluded that (1) the mean apparent speed is already 800 km/s at 10 R_S and probably even at 5 R_S; also (2) the apparent radial speed of the polar wind exhibits great "spatiotemporal fine structure" and is not well described as a smooth, spherically diverging flow. The vertical spread in points around a given radius represents the true flow speed dispersion. The dotted horizontal lines are the upper and lower bounds of Ulysses measurements over the polar regions.

Each of these three hypotheses is closely related to an associated process for the cause of high-speed wind. Solar Probe will pass through precisely the most important heights in coronal holes for distinguishing between these possibilities. Therefore, the mission will be well situated to analyze the acceleration physics associated with this phenomenon and its relationship to the production of the smaller-scale turbulent fluctuations observed in the high-speed wind by Ulysses.

Next, SOHO's Large Angle and Spectrometric Coronagraph (LASCO) has directly confirmed something suspected for many years but difficult to observe—that the flow in coronal holes is indeed far from homogeneous. Figure 7 (left panel) is a contrast-enhanced portion of a LASCO C2 image (2.0 to ~4.0 R_S). This image shows bright rays in the coronal holes, delineated by the horizontal white bars. These plumes are bright because they are denser than the surrounding interplume plasma. One of the first Joint Observing Programs on SOHO (JOP 39) focused specifically on polar regions and plume flows. The conclusion of that and later studies is that plumes exist in all coronal holes. Plumes lie over magnetic flux concentrations in the photosphere, although not all flux concentrations have plumes. We do not understand how plumes are created or how the higher density is supported. Not only will Solar Probe pass directly through this field of plumes at ~5 to 10 R_S, but also the coronal imager on Solar Probe will be able to make close-up pictures of plumes, and the photospheric imagers will be able to analyze the differences in magnetic field structure in individual magnetic flux concentrations.

It is not surprising that plumes exist in coronal holes, because the ratio of thermal energy density to magnetic field energy density $\beta << 1$ out to at least 10 R_S (Suess and Smith, 1996), and there is thus little dynamic interaction of plasma across magnetic flux tubes in this region. The photospheric magnetic field in general, and magnetic flux concentrations in particular, are highly irregular in size, shape, amount of mixed magnetic polarity, and temporal variations. Plumes probably form over those concentrations that

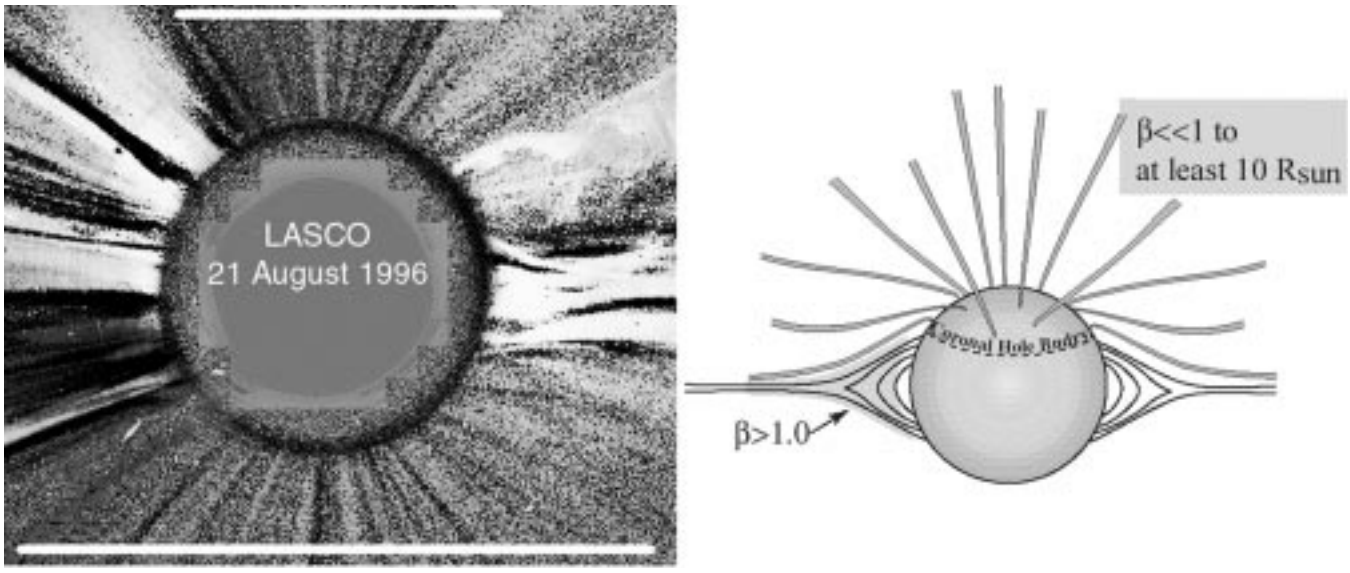

Figure 7. *Left*: A SOHO/LASCO C2 image that has been digitally enhanced to bring out the radial striations in the polar coronal holes. Radius of the occulting disk is 2 R_S. White bars at the top and bottom of the image delineate the regions containing the striations. These are plumes, the bright ray-like structures that have been known for many years. *Right*: Schematic of coronal streamers and coronal holes emphasizing the empirical result that the plasma β (ratio of thermal energy density to magnetic field energy density) is small in coronal holes and greater than unity in streamers. Plumes are illustrated in the coronal hole where they can exist primarily as a consequence of $\beta << 1$. Beyond ~10 R_S, β approaches unity and plumes are observed to become diffuse and difficult to detect with LASCO.

have opposite polarity flux being pushed into the concentration by photospheric motions. The resulting magnetic reconnection apparently heats the base of plumes and increases the overlying density, but we do not yet understand how plumes are maintained. Because of the highly variable photospheric field, however, the footpoints of field lines extending into the corona have strongly varying conditions. These differing conditions will not communicate to nearby flux tubes because $\beta << 1$ just above the chromosphere. The heating at the base of a plume may raise the density in the overlying flux tube, but the adjacent flux tube is unaffected. Thus, it can be anticipated that filamentary plasma structures will exist in coronal holes down to the smallest scale of the photospheric magnetic field, which is probably no larger than ~100 km. One important measurement possible with Solar Probe will be to relate the dispersion, or fine structure, in the solar wind proton temperature (Figure 4) to *in situ* coronal temperatures. This information will allow us to identify dynamic processes from the imprint of this fine-scale photospheric magnetic field structure.

The flow speed in plumes has been shown by the Doppler dimming measurements of SOHO/UVCS to be ~130 km/s at ~2 R_S (Corti et al., 1997), which can be used with empirical plume densities and inferred geometry to estimate plume flow speed at 5.5 R_S. Plume geometry is known because of the low β of the plasma (Suess et al., 1998). There is rapid divergence (observed with SOHO's Extreme Ultraviolet Imaging Telescope/EIT) up to a height of ~50,000 km, and then above 50,000 km plume and interplume flow tube geometries are essentially identical. Assuming the flows are identical, the flow speed in plumes is found to be 130–230 km/s at 5.5 R_S. Comparing this range of speeds with the measured speeds shown in Figure 6 (which shows that the mean apparent speed of the solar wind is 500–750 km/s at 5.5 R_S), it can be seen that plumes flow at less than half the speed of interplume plasma. This dichotomy in speeds means that plumes would be expected to stand out clearly in Ulysses data. Several searches have been made of high-latitude Ulysses data for plume-like signatures, and an earlier search was made of Helios data (Marsch, 1991), with only tentative

identifications at best. There are identifiable structures in the fast wind, including the "pressure balanced structures" of McComas et al. (1995) and the "microstreams" of Neugebauer et al. (1995), which may be the residue of plumes and other phenomena, but the absence of an obvious signature shows that plume and interplume plasma must undergo mixing somewhere between ~10 and 20 R_S, where plumes begin to fade in LASCO images, and ~0.3 AU, where they have no obvious signature in the Helios data. At present, the only possible way of analyzing the plasma processes in this region is through the use of *in situ* measurements. Solar Probe's prime mission covers this region.

Figure 8 shows data collected to observe flow in plumes during the SOHO JOP 39. These are the data used to show the co-alignment of plumes and some magnetic flux concentrations. The bases of plumes are visible in the center panel as enhanced emission, while the magnetic flux concentrations are visible in the magnetogram in the top panel. JOP 39 also revealed that magnetosonic waves often propagate up (away from the Sun) in plumes and are visible because of the enhanced density.

The bottom panel of Figure 8 shows macrospicules extending up through the transition region, sometimes reaching heights of 100,000 km and speeds of 150 km/s. This impulsive phenomenon is like a piston in a rigid tube at these heights, again because $\beta << 1$. It should produce shocks and local heating of the plasma in the flux tubes and may accelerate particles. This jet-like phenomenon may be a consequence of reconnection in the photosphere. Somewhat larger-scale jets have been well observed in active regions by Yohkoh, and models of the process, such as that shown in Figure 9, have been developed. Small-scale activity (microflares) occurs in the network and appears to be the source of the energy required for the solar wind, but we do not know how this energy is transferred to the solar wind. It can be transported in the form of waves, jets, and perhaps energetic particles that could all be detected at 4 to 8 R_S. Virtually all the strong (kilogauss) magnetic flux elements not in sunspots or pores are concentrated in the network, at scales as small as ~100 km. Diffuse bipoles are continuously swept into these regions and must be replenished. The primary tasks

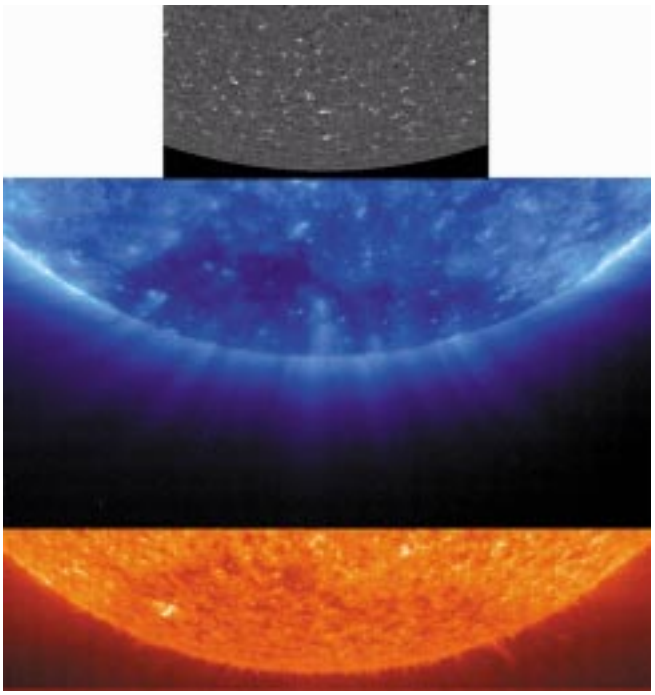

Figure 8. South polar images made during JOP 39 to study polar plume flow. *Top:* Magnetogram (SOHO/MDI) showing the dominant (white) polarity in the south polar coronal hole with flux occurring mostly in strong flux concentrations. *Center:* FeIX/X 171 Å emission (SOHO/EIT) showing the base of plumes and bright points. *Bottom:* He 304 Å emission (EIT) showing macrospicules and chromospheric network, and the southern polar coronal hole.

of a photospheric imager on Solar Probe are (1) to determine the size and temporal evolution of magnetic flux elements as a function of solar latitude and type of Sun (quiet, active, plage, and coronal hole) and (2) to determine the size and interaction rates of magnetic reconnection like that of Figure 9.

SOHO spectroscopic observations have revealed other surprising properties of the solar wind in coronal holes in the first few solar radii above the solar surface. SOHO/UVCS line profiles were found to have a component with a very large width. This is shown in Figure 10 for the HI Lyman α line. Oxygen lines are even more extreme, with a higher $v_{1/e}$ (equivalent velocity half-width). These widths are larger than the expected outflow speed at these altitudes; the cause is probably not simple turbulence, since H^0 has smaller widths than O^{5+}. Also, a plasma in thermodynamic equilibrium with the observed

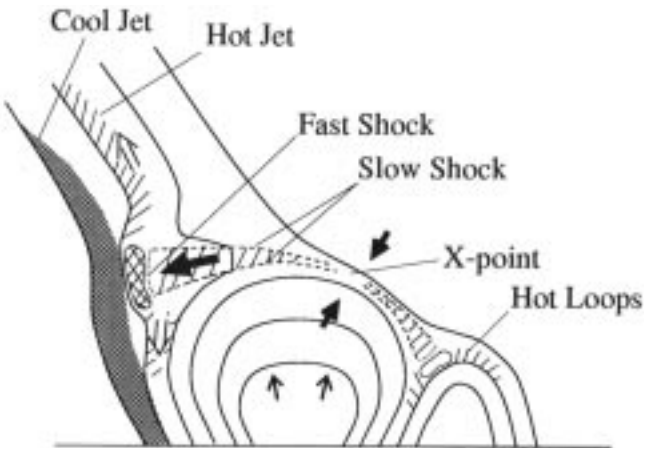

Figure 9. Schematic of physical processes found from numerical simulations of magnetic reconnection associated with emerging flux. The solid lines represent magnetic loops, which become interconnected and release energy to heat plasma and form jets (Yokoyama and Shibata, 1996).

$v_{1/e}$ for OVI 1037 at 2.1 R_S would have a temperature of 2.3×10^8 K, which is much larger than the freezing-in temperature measured by the Solar Wind Ion Composition Spectrometer (SWICS) on Ulysses. If this higher temperature were interpreted as the line width in the radial direction, it would also be so broad that no Doppler dimming would be observed (Corti et al., 1997). Therefore, since Doppler dimming is observed, the conclusion is that the line widths are less in the radial direction, and that the large $v_{1/e}$ is probably due to damping of ion-cyclotron waves or Alfvén waves. This hypothesis should be considered in light of the results shown in Figure 5 for the proton temperature anisotropy in the solar wind.

Clearly, very interesting processes are occurring between 4 R_S and the interplanetary medium, but what they are is truly completely unknown. Just as clearly, these processes have something to do with how energy is deposited in fast solar wind. Solar Probe will determine the wave amplitudes in the corona, how the waves vary from one flux tube to another, and the type of waves present. Figure 11 collects results of the type shown in Figure 10 and plots them versus height. In coronal holes, the 1/e velocities of O^{5+} begin to rise above HI at ~1.6 R_S, suggestive of ion-cyclotron wave heating. This difference apparently continues to grow with increasing height, and there is a strong mass-to-charge dependence of temperature in the solar wind. In streamers, the behavior of HI and O^{5+} is completely different, and the 1/e velocities become equal only at ~5 R_S. Again, Solar Probe will be in the right place to collect data on this phenomenon.

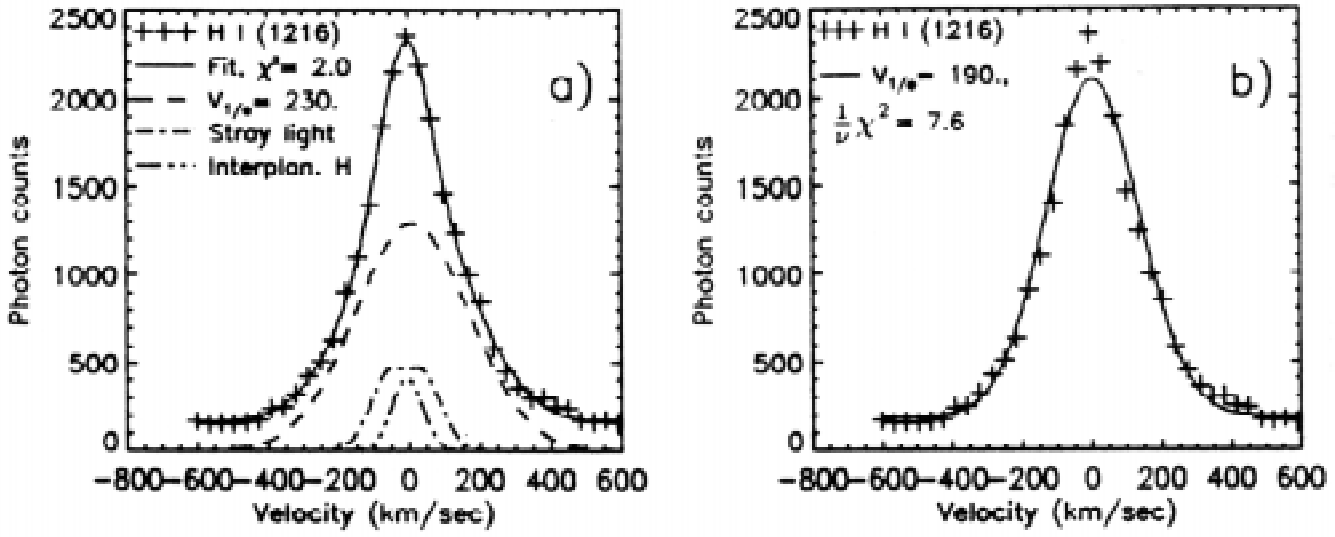

Figure 10. HI Lyα profiles for the south polar coronal hole at 3.0 R_S observed on 11 May 1996 from SOHO/UVCS. Computer fits for a single Gaussian plus a constant (b) and three Gaussians plus a constant (a) are shown. The narrow component corresponds to a kinetic temperature of O[10^6] K ($v_{1/e}$ ~ 130 km/s). The broad component corresponds to $v_{1/e}$ ~ 240 km/s and includes the effects of both thermal and nonthermal motions (Kohl et al., 1997).

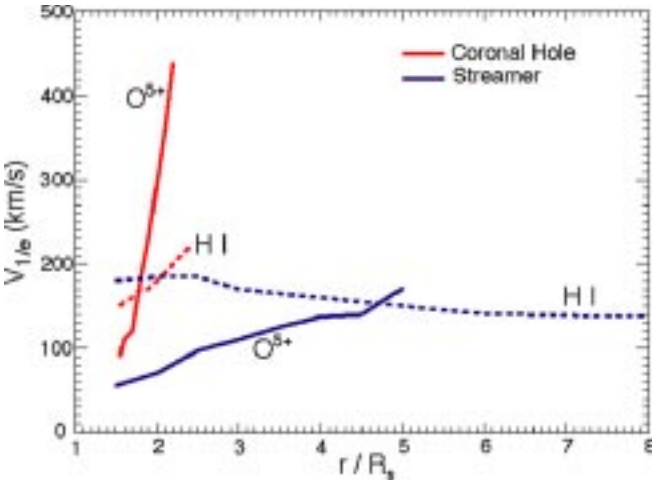

Figure 11. Line widths as a function of height for H and O, showing the divergence above 1.6 R_S in coronal holes. This divergence requires the waves producing the perpendicular temperature to be driven at these heights (Habbal, private communication).

What we know of coronal hole flow as a consequence of SOHO and other remote observations:

- Flow at 4 to 10 R_S is highly variable.
- Flow at 4 to 10 R_S is highly filamented.
- Perpendicular kinetic temperatures are large and vary from ion species to ion species.

What needs to be answered with Solar Probe:

- How does the variable, filamented flow become the uniform flow (in speed) that we see in the solar wind?
- What causes the high perpendicular kinetic temperature, and what is its relation to ion heating in coronal holes and streamers?
- At what height and how does heating occur?

2.4 Remote Sensing of the Corona and Photosphere—Slow Wind, Streamers, and the Solar Probe

The principal origin of slow wind is believed to be streamers, as described in Section 2.1. Slow wind may be stripped off the flanks of streamers, may leak out of the tops of streamers, may be released by reconnection of magnetic field lines at the base of streamers, or may result from some combination of these processes. Streamers and coronal holes present radically different conditions, which is undoubtedly the reason they produce slow wind (and possibly some fast wind in filamentary structures embedded in streamers), the reason they are the location where CMEs occur, and therefore the reason they are an important Solar Probe objective.

As a consequence of Yohkoh and SOHO observations, the ambient conditions in streamers are far better known than they were just 5 years ago. The plasma density and electron temperature T_e (but probably not proton and ion temperatures) are higher than in coronal holes at similar heights. UVCS results imply that proton temperature $T_p \sim T_e$ in streamers and that the temperature varies only weakly with height. The plasma contained in closed magnetic field regions should be roughly in hydrostatic equilibrium, with all energy inputs and outputs in balance. This implies that radiative losses may be important. If energetic particles are accelerated near or in the chromospheric network, they may remain trapped for relatively long periods in closed magnetic field regions.

Dynamic motions in streamers present a more difficult observational problem. Figure 12 shows a CME observed by LASCO. This corkscrew-shaped ejection moved at a few hundred kilometers per second between 2 and 6 R_S and was several times more dense than the ambient. It is suspected that the magnetic field and the plasma were equally contorted in this image, although this can only be inferred. The morphology will be especially difficult to understand at solar maximum, during the first Solar Probe perihelion passage, when CMEs like this are common. There will also be contributions from shocks upstream of CMEs and from flares to the energetic particle populations. However, combining vector magnetic field measurements with particle measurements and tomographic imaging would give a powerful tool for resolving the ambiguities.

The elemental composition in streamers is expected to be a particularly important diagnostic tool for slow wind origins and for determining the physics of streamer confinement. This possibility is already suggested by the charge-state and freezing-in temperature differences in the slow wind illustrated in

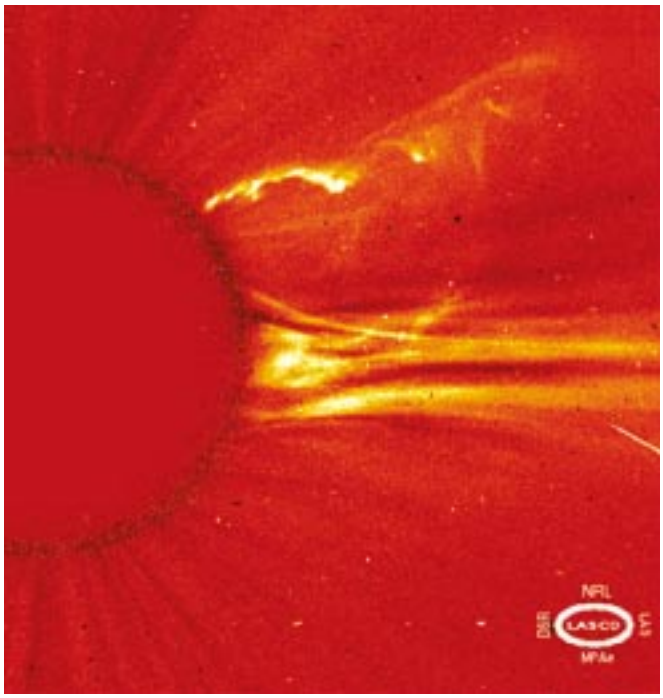

Figure 12. Corkscrew CME observed on 21 August 1996 with the SOHO/LASCO C2. Such CMEs occur several times per day near solar maximum.

Figure 3. Raymond et al. (1998) used SOHO/UVCS to measure the composition in streamers; they reported that gravitational settling produces an overall depletion of heavy elements at large heights in closed-field regions and that this settling is greater in the core of streamers than on the flanks. They showed that if the legs were static, the abundance would be less than in the central part of the streamer. Since the opposite is the case, streamer legs are not static and are therefore the probable source of slow wind. They speculated that the enhancement of heavy elements in streamer legs results from some form of mixing that refreshes the material in the legs on a time scale of 1 day or less. This, and all other suggested processes for release, ejection, or evaporation of slow wind from streamers, would be reflected in the details of gravitational settling and, as a consequence, the composition.

To determine how slow wind is produced, we need to understand streamer confinement. Confinement depends on the bulk plasma properties and magnetic fields, both in streamers and in surrounding coronal holes. A recent empirical result is that $\beta > 1$ above ~1.2 R_S in one streamer (Li et al., 1998). It will be important to understand whether this result is typical of streamers or whether it is true only near the tops of streamers.

If $\beta > 1$ throughout streamers, then the magnetic field in surrounding coronal holes must provide the main confinement force. Conversely, if $\beta < 1$ everywhere except near the tops of streamers, the curvature force of the streamer magnetic field can provide the main confinement, and leakage of slow wind from inside streamers is less likely. Solar Probe will answer this question by measuring composition and bulk plasma properties at the tops of streamers and determining *in situ* magnetic field to give the local value of β across the top of the streamer and in the adjacent quiet corona and open field regions.

What we know of streamers and slow wind origins as a consequence of SOHO and other remote observations:

- Elemental abundances vary across streamers.
- Temperatures are more isotropic in streamers than in coronal holes.
- Flow speeds are less above streamers than in coronal holes.

What needs to be answered with Solar Probe:

- How do proton and electron heating and temperature vary?
- How does slow wind escape from streamers?
- What are the energetic particle populations, wave–particle interactions, and trapping efficiency?

2.5 Solar Probe in Context

Figure 13 shows a model prediction for the appearance of the corona during the February 1998 total solar eclipse with the Solar Probe orbit overlaid for comparison. The model suggests that Solar Probe will pass through the corona just at the tops of closed loops in streamers. Otherwise Solar Probe will be on open field lines unless it encounters a CME. The local geometry of the magnetic field and the ambient plasma properties should show if a CME is encountered. Trapped particles should be absent on open field lines. At the tops of streamers the flow

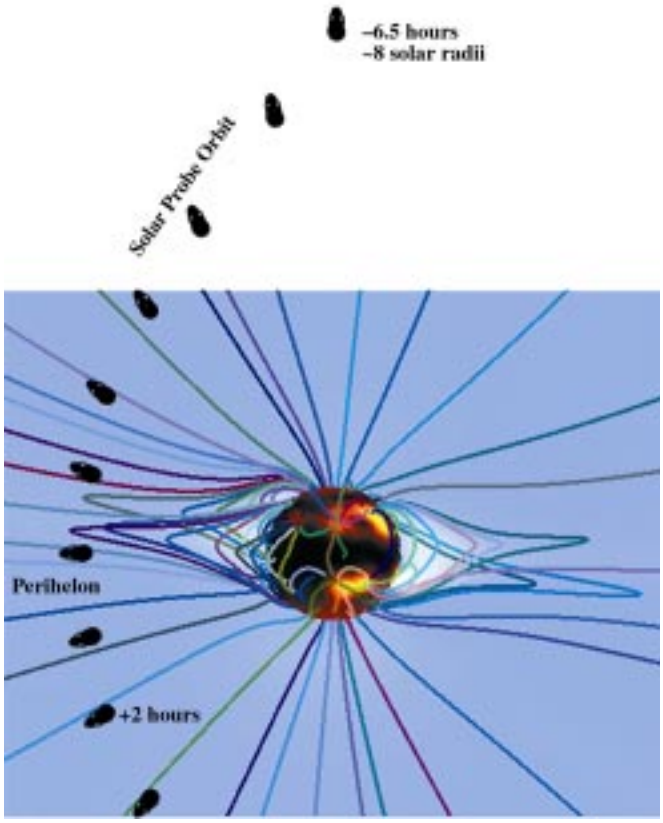

Figure 13. Prediction of the white light corona and coronal magnetic field for the 26 February 1998 total solar eclipse (J. Linker and Z. Mikic, private communication). Photospheric magnetic field data from Carrington rotations 1931–1932 (January 18–February 12, 1998) from the National Solar Observatory were used as a boundary condition. Superimposed is the Solar Probe trajectory. According to this model, Solar Probe will be just at the tops of closed loops.

speed will be subsonic, giving probably the only chance Solar Probe will have to sample subsonic wind.

Conversely, in coronal holes (outside plumes) the average bulk properties lie within reasonably well-defined bounds. Figure 14 shows coronal hole properties derived empirically or from one-, two-, and multifluid models. The flow speeds are essentially like those shown in Figure 6. On the basis of SOHO results, the models assume that, in coronal holes, $T_e < T_p$ (and less than the temperatures of heavier ions) and that the temperatures are strongly anisotropic. These properties depend on how plasma is being heated. Physically, the flow speed is sub-Alfvénic inside ~10 R_S and therefore Alfvén waves will propagate both inward and outward relative to the Sun. This flow pattern affects the energy balance and is an important reason for Solar Probe's perihelion to be inside 10 R_S.

Solar Probe *in situ* measurements will sample only a small volume of plasma. To correlate these measurements with ambient structures, white-light measurements of the corona are planned. The steadily varying perspective of wide-field images taken throughout the encounter will allow reconstruction of global structures. The objectives are to create a 3-dimensional image of these structures and to probe filamentary structures (Figure 7) with unprecedented resolution. At the same time, of course, the mission will obtain the first view of the longitudinal structure of the corona from over the solar poles. Solar Probe will make images and, by differencing and tomography, provide the context for what it encounters. Solar Probe will also fly through streamers, where remote imaging is extremely limited by line-of-sight effects. Anticipating what we will observe there is difficult, but the high spatial resolution, combined with the ability to gain perspective with a rapidly changing viewing angle, will enable determination of the 3-dimensional properties of streamers in detail far beyond what is possible from 1 AU.

A Solar Probe photospheric imager can analyze the dynamics of small magnetic flux elements in the photosphere and provide information for determining the context of Solar Probe global coronal measurements. One of the most important observations is to provide a proper boundary condition for the global field used in model predictions and analyses such as that shown in Figure 13. The polar field is extremely difficult to measure from the ecliptic plane because it is being viewed at a very shallow angle. Solar Probe will look directly down on the poles. The observations also will allow helioseismological analysis of measured Doppler velocities. Such analysis can confirm some of the SOHO/Michelson Doppler Imager's (MDI's) most important discoveries about the solar interior, including (1) whether the rotation rate at higher latitudes is 10–20% lower than was expected before MDI; (2) whether there is a polar vortex; (3) whether small- and large-scale magnetic fields on the Sun are rooted at different depths in the

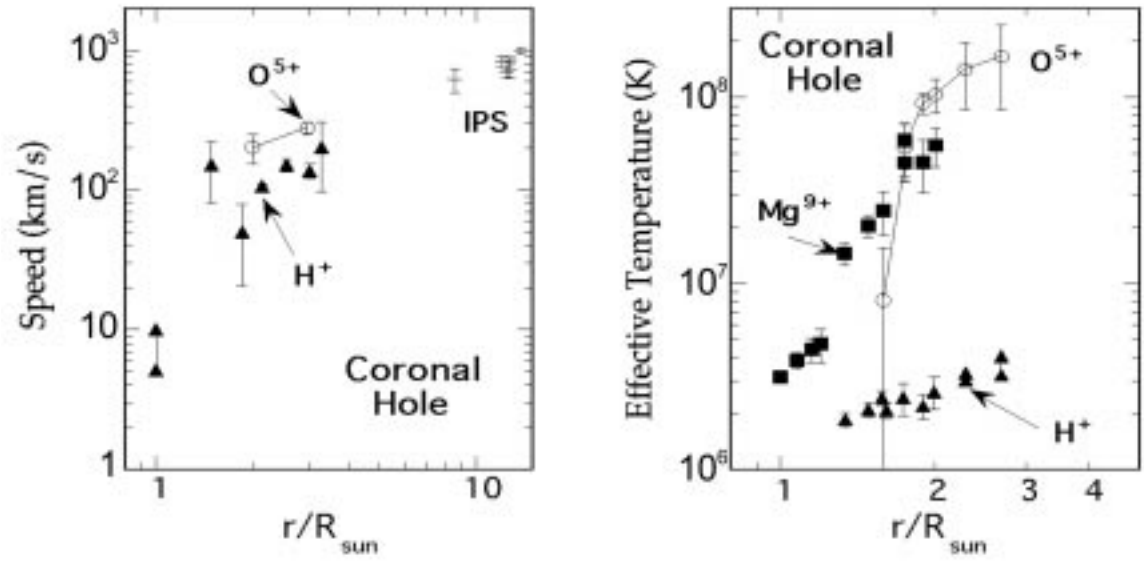

Figure 14. Parameters of the initial solar wind inferred from model calculations and remote sensing of coronal holes. In the left panel, the speeds of protons (filled triangles) and of oxygen (open circles) are from SOHO/UVCS measurements (Kohl et al, 1997), as are the effective temperatures for the indicated ions in the right panel. The observations show that fast solar wind is still being accelerated and is slower than its ~750 km/s terminal speed at 4 R_S. Also, the effective temperature of heavy ions (Mg and O) is greater than that of protons.

convection zone; (4) whether surface and subsurface meridional flows are as high as estimated with MDI; and, finally, (5) what the magnitude and distribution of polar magnetic flux are. The magnitude has variously been estimated between 2 and 20 G, varying between cos θ and $\cos^8 \theta$ (where θ = colatitude) in independent measurements.

The possible concentration of magnetic flux at the poles of the Sun may be related to the "polar vortex" shown in Figure 15. MDI measurements of the polar regions, which are limited in resolution because of the oblique observing angle, indicate a circumpolar jet stream within 15° of the pole. The jet is believed to be relatively shallow, extending only to ~20,000 km below the visible surface. There are weaker indications that the polar vortex extends to the bottom of the convection zone.

What we know of the coronal context as a consequence of SOHO and other remote observations:

- There is unresolved filamentary flow in coronal holes.
- Streamers extend well beyond 4 R_S with subsonic flow at the tops.
- Coronal hole boundaries are extremely sharp.
- The polar regions of the Sun have different rotational and magnetic field properties from the equator.

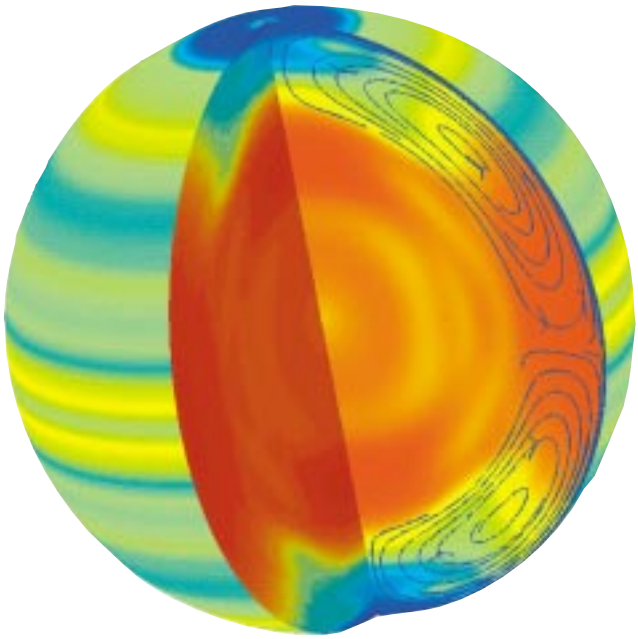

Figure 15. The Sun rotates much faster at the equator than at the poles. However, SOHO/MDI has revealed belts where there are differential flows. In particular, there is a "vortex," shown here in deep blue, situated over each pole (Schou et al, 1998).

What needs to be answered with Solar Probe:

- What are the absolute value and variability of flow at streamer tops?
- What is the minimum scale of coronal hole filamentary structure?
- What is the relationship between coronal hole boundaries and the magnetic field?
- What are the relationships among solar rotation, polar magnetic field, and coronal holes?

2.6 Synopsis

Solar Probe addresses the many, sometimes contradictory, ideas about the source of the solar wind and, by extrapolation, of stellar winds. Solar Probe will resolve the questions about extended heating versus basal heating, for example; about waves versus pulsed solar wind versus jets versus particle beams; about mixing of the fast solar wind with embedded filamentary structures; about temperatures and temperature anisotropies of heavy elements; and about MHD wave and plasma wave roles. Data from Solar Probe will answer many of the questions raised by these ideas—ideas arising from missions sponsored by NASA, the European Space Agency (ESA), and Japan's Institute of Space and Astronautical Science (ISAS), as well as from a long history of ground-based observations of the Sun.

As noted in Section 3, the Solar Probe Science Definition Team was charged with defining and categorizing the prime scientific objectives for the mission. Listed below are the primary (category A) and secondary (category B/C) science questions addressed by Solar Probe, along with synopses of how the mission answers each question.

How Solar Probe answers the primary science questions (category A questions):

- *Determine the acceleration processes and find the source regions of fast and slow solar wind at maximum and minimum solar activity.*

  Using two passes through the corona—at maximum and minimum solar activity and at the height of streamer tops and heating and momentum deposition in coronal holes—Solar Probe will make the measurements needed for analysis of the physics of acceleration in the slow and fast wind source regions. Measurements are needed of the vector magnetic field and of the electron and proton velocity, density, and parallel and perpendicular temperature at sufficiently high time resolution to resolve the finest expected scales (~100 km at the photosphere). Ion composition is needed at least for He, O, Si, and Fe for comparison with the observations from Ulysses and SOHO. Plasma wave measurements will be necessary to resolve the wave modes, directions of propagation, any nonlinear effects, and forms of particle heating. Energetic particle measurements will be needed to determine sources and trapping mechanisms, as well as to infer from their measured properties the physical conditions of the plasma and magnetic fields in the regions where they are accelerated and through which they propagate. The suggested instruments and their properties meet these requirements.

- *Locate the source and trace the flow of energy that heats the corona.*

  Measurements from 4 R_S out to at least 30 R_S are needed to explain the relationship and large differences known to exist between coronal and solar wind properties. Heating is a function of height and ambient properties, which can only be resolved physically with a knowledge of radial evolution.

- *Construct the 3-dimensional coronal density configuration from pole to pole, and determine the subsurface flow pattern, the structure of the polar magnetic field, and its relationship with the overlying corona.*

  Imaging of the surrounding corona as Solar Probe passes from pole to pole, in combination with *in situ* measurements of the bulk plasma, will produce contextual images of the corona and the first polar view of the equatorial corona. Our understanding of streamer morphology also will be enormously improved. Photospheric imaging from a polar perspective will confirm or reject the proposed polar solar rotation vortex and a (possibly associated) polar peak in magnetic field strength.

- *Identify the acceleration mechanisms and locate the source regions of energetic particles, and*

determine the role of plasma waves and turbulence in the production of solar wind and energetic particles.

Energetic particle measurements will be made in combination with vector magnetic field measurements to define regions of local particle trapping and photospheric origin of particles. Analysis of energetic particle data will be used to remotely probe and characterize the plasma and magnetic structure. High-time-resolution plasma measurements necessary for defining the limits of filamentation in coronal holes will also enable definition of the evolving field of MHD turbulence with increasing heliocentric distance.

How Solar Probe answers the secondary science questions (category B and C questions):

- *Investigate dust rings and particulates in the near-Sun environment.*

  Dust and particulates accumulate near the Sun by condensation out of coronal gasses and infall from the interplanetary medium. An enhanced concentration is expected to exist outside 4 R_S, and Solar Probe is the only proposed mission capable of demonstrating its existence. The distribution of dust and its composition can be inferred from observation of pickup ions using the same instrument that measures the composition of the solar wind. The impact of large dust grains can be recorded by the plasma wave instrument.

- *Determine the outflow of atoms from the Sun and their relationship to the solar wind.*

  Determining the composition of coronal plasma is one of Solar Probe's prime objectives. The same instrument that measures composition can also measure outflow, producing a valuable addition to the body of information used to analyze acceleration and heating.

- *Establish the relationship between remote sensing, near-Earth observations at 1 AU and plasma structures near the Sun.*

  Remote sensing observations from 1 AU cannot resolve the fine structure in coronal holes, and they are limited by line-of-sight effects in streamers. Nevertheless, a large body of data being recorded now by SOHO, ACE, Wind, and Ulysses and taken over the past decades may contain unexpected and useful information if placed in the context of *in situ* and imaging measurements from Solar Probe.

- *Determine the role of X-ray microflares in the dynamics of the corona.*

  X-ray microflares occur in the chromospheric network as magnetic bipoles advected into the network from supergranule interiors. The photospheric imaging experiment may help to determine whether X-ray microflares are the source of some coronal jets. The energetic particle instrument may detect related particle acceleration.

- *Probe nuclear processes near the solar surface from measurements of solar gamma rays and slow neutrons.*

  The addition of a gamma-ray and slow neutron detector would enable the determination of sources in the photosphere that are associated with microflares and other small-scale photospheric activity.

3. Instrument Payload Required to Address Prime Science Objectives

The Solar Probe Science Definition Team was charged with defining the prime scientific objectives for the Solar Probe mission and establishing a core "strawman" instrument payload to address these objectives. The Team prioritized the science objectives in three categories:

- *Category A* —Irreducible core objectives to be fulfilled with the baseline instrument payload
- *Category B* —Objectives that would require a minimal enhancement to the core payload
- *Category C*—Objectives that could be addressed with additions to the core payload

The Science Definition Team also identified payload and measurement requirements, including nadir viewing for the plasma and remote sensing instruments viewing the solar surface. The core payload requirements were then used for the baseline spacecraft and mission design.

3.1 The Prime Scientific Objectives of the Solar Probe Mission

Category A science objectives:

- Determine the acceleration processes and find the source regions of the fast and slow solar wind at maximum and minimum solar activity.
- Locate the source and trace the flow of energy that heats the corona.
- Construct the 3-dimensional coronal density configuration from pole to pole, and determine the subsurface flow pattern, the structure of the polar magnetic field, and its relationship with the overlying corona.
- Identify the acceleration mechanisms and locate the source regions of energetic particles, and determine the role of plasma waves and turbulence in the production of solar wind and energetic particles.

Category B science objectives:

- Investigate dust rings and particulates in the near-Sun environment
- Determine the outflow of atoms from the Sun and these atoms' relationship to the solar wind.
- Establish the relationship between remote sensing, near-Earth observations at 1 AU and plasma structures near the Sun.

Category C science objectives:

- Determine the role of X-ray microflares in the dynamics of the corona.
- Probe nuclear processes near the solar surface from measurements of solar gamma-rays and slow neutrons.

3.2 Science Implementation

The measurement requirements follow from the science objectives. The strawman payload was selected on the basis of a combination of measurement requirements and mission and spacecraft constraints. The requirements of the thermal environment and the Jupiter gravity assist, as well as the need to use the smallest launch vehicle consistent with the mission (to minimize program costs), force severe mass and power constraints on the spacecraft and science payload. Hence the payload must be capable of returning the required measurements while being commensurate with the smallest impact on spacecraft resources. Recent technological innovations in reducing instrument mass and power enable such a payload to be identified.

3.3 Measurement Objectives

To determine acceleration processes and source regions for fast and slow solar wind at solar minimum and maximum requires (a) a full suite of plasma state measurements (distribution functions, composition, magnetic field, and wave spectra) and (b) remote sensing to set the context of the *in situ* measurements both locally and globally. These measurements can be achieved with a Solar Wind Particle and Composition Spectrometer, an Energetic Particle Composition Spectrometer, a Vector Magnetometer, and a Plasma Wave Sensor.

The Energetic Particle Composition Spectrometer fills in the suprathermal part of the plasma distribution functions. In combination with plasma wave measurements, it identifies accelerated particle characteristics as diagnostics for plasma turbulence and for wind dynamics at lower altitudes than directly sampled by the probe. A Fast Solar Wind Ion Detector resolves ion characteristics on the scale of an ion gyroperiod, in conjunction with the Plasma Wave Sensors, to examine the role of wave–particle effects in the acceleration (and heating) of the wind. Slow and fast solar wind regions are sampled by the polar trajectory of Solar Probe, while sampling near both minimum and maximum solar activity periods is achieved by the two perihelion passes separated by about 5 years.

Actually matching up *in situ* measurements with distinct surface features is problematic; however, the magnetic field beneath the trajectory as well as the temperature and density structure are required for setting the context of the wind through which the probe is flying. A Visible Magnetograph and Extreme Ultraviolet (XUV) Imager fulfill these requirements. The more local environment through which the probe is flying is characterized by an All-Sky, 3-Dimensional Coronagraph Imager that can identify the larger structures that are being locally sampled by the *in situ* science instruments.

Locating the source and flow of energy that heats the corona requires the same instrument set. Very likely, the acceleration of the solar wind and the heating of the corona are intimately linked. The Vector Magnetometer and Energetic Particle Spectrometer will link the *in situ* measurements along the magnetic field back toward the Sun with the regions sampled by the Remote Sensing Package. By looking for remote features that can be linked with *in situ* measurements, e.g., the heat flux in the various ion distributions, the connection between photospheric dynamics and coronal energetics can be established.

Constructing the 3-dimensional density configuration from pole to pole, determining the subsurface flow pattern, and determining the structure of the polar magnetic field and its relationship with the overlying corona require the instruments in the Remote Sensing Package.

The acceleration mechanisms of energetic particles are identified, their source regions are located, and the role of plasma turbulence in the production of solar wind and energetic particles is determined with the Energetic Particle Composition Spectrometer operating with the Fast Solar Wind Ion Detector and Plasma Wave Sensor.

3.4 Strawman Payload and Observational Approach for the Solar Probe Mission

The strawman payload developed by the Solar Probe Science Definition Team is one conceptual design that allows Solar Probe to meet all of the category A science objectives. It represents one possible implementation solution based upon near state-of-the art engineering capabilities at the concept-design level. The mass, power, and data-rate allocations do not represent a unique solution; however, they do show the types of trade-offs required to assemble a complete payload on such a resource-constrained mission (e.g., Axford et al., 1995; McNutt et al., 1996a; Tsurutani et al., 1997). Technology advances, especially in electronics miniaturization, suggest that payload mass can be reduced by more than a factor of ~6 from designs of a decade ago to address science questions that have remained essentially unchanged (Feldman et al., 1989).

Solar Probe's category A measurement objectives can be met with a strawman payload consisting of five *in situ* and three remote-sensing miniaturized instruments. Table 2 lists quantitative details of the measurements required to address the category A science objectives for each instrument. Table 3 lists the spacecraft resources required to accommodate each instrument. With this configuration, the total mass and power for the strawman payload are under 19 kg and 16 W, respectively. These numbers do not include allocations for the two data processing units (DPUs). The system flight computers are expected to provide the science data processing normally performed by the DPUs (see Section 5.3). The data rate at the time of closest approach is over 112 kilobits per second (kbps), roughly half of which will be transmitted in real time, with the rest stored onboard for transmission after the perihelion passages (see Section 4.2).

The most economical use of these resources is achieved by configuring the instruments into two instrument packages to provide organizational integration and to reduce programmatic complexity: (1) the *In Situ* Science Package, consisting of a Vector Magnetometer, Solar Wind Ion Composition and Electron Spectrometer, Energetic Particles Composition Spectrometer, Plasma Wave Sensor, and Fast Solar Wind Ion Detector; and (2) the Remote Sensing Package, consisting of a Visible Magnetograph Helioseismograph, an XUV Imager, and an All-Sky, 3-Dimensional Coronagraph Imager.

In this strawman payload, sampling techniques are mentioned only to indicate that at least one possible solution exists for science implementation. The architecture of the integrated packages is not described. We provide a guide showing how investigations could respond to the science objectives using instruments with particular choices of spectral range and resolution, sensitivity and dynamic range, field-of-view range and angular resolutions, and time and spatial resolution. The measurement requirements listed in Table 2 are example parameters for a credible payload.

Table 2. Strawman instrument payload for Solar Probe: measurement requirements.

Strawman Instruments	Parameter(s) or Quantity(ies) Measured	Sensitivity, *Dynamic Range*	Spectral Range, *Resolution*	Angular Range, *Resolution*	Time or Spatial Resolution
		In Situ Science Package			
Vector Magnetometer	Vector DC magnetic field	±0.05 nT *10^3*	—	—	10 ms 3 km
Solar Wind Ion Composition and Electron Spectrometer	Dist. functions of dominant charge states of H, He, C, O, Ne, Si and Fe; electrons	10^5/cm^{2}s *$2 \cdot 10^7$*	0.05 < E < 50 keV/e *$\Delta E/E < 0.07$*	Nadir ±20° and 135° × 300° *$10° \times 10°$*	1 s for H, He, e$^-$; 10 s for heavy ions
Energetic Particle Composition Spectrometer	Differential fluxes of H, ^{3}He, ^{4}He, C, O, Si, Fe, and electrons	10/cm^{2}s sr keV *10^7*	0.02 < E < 2 MeV/n e$^-$: 0.02–1.0 MeV *$\Delta E/E < 0.07$*	135° × 300° *$20° \times 20°$*	1 s for e$^-$; 5 s for H 30 s for heavy ions
Plasma Wave Sensor	AC electric and magnetic fields	10^{-5} V/m 10^{-9} nT/Hz *10^6*	0.05–150 kHz *$\Delta\omega/\omega = 0.05$*	—	1 ms (wave cap) 1 s (spectral)
Fast Solar Wind Ion Detector	Dist. functions of ions	10^6/cm^{2}s *10^6*	0.02 < E < 50 keV/e *$\Delta E/E < 0.07$*	90° × 300° *$10° \times 10°$*	1 ms
		Remote Sensing Package			
Visible Magnetograph–Helioseismograph	Magnetic field, line-of-sight velocity field, intensity	10 G *300* 20 m/s *400* 1% *400*	3 Å visible *70 mÅ*	1024 arc-sec *2 arc-sec*	2 s 32 km
XUV Imager	Intensity @ entrance aperture	100 ergs/cm^2 sr *400*	EUV Band providing coronal imaging, *8Å*	2560 arc-sec *5 arc-sec*	<1 s
All-Sky, 3-Dimensional Coronagraph Imager	White light	Signal to noise >100, *>1000*	400–700 nm	20–180° from S/C–Sun line *<1°*	<1 min

The *In Situ* Science Package:

Vector Magnetometer. Precise and accurate measurements of the orientation and intensity of the coronal magnetic field are essential to the achievement of all category A science objectives. Knowledge of the large-scale coronal magnetic structure is fundamental to the modeling and analysis of solar wind flow and energetic particle transport. On shorter scales, the magnetic field is diagnostic of the rate of magnetic dissipation in regions where reconnection is taking place, the structure of current sheets and other types of discontinuities, the properties of helical magnetic structures such as flux ropes, and the propagation characteristics and strength of shock fronts. Finally, low frequency (<1 Hz) MHD waves must be accurately detected and analyzed to assess their role in solar wind heating and acceleration.

Table 3. Strawman instrument payload for Solar Probe: instrument requirements.

Strawman Instruments	Mass* (kg)	Power* (W)	Data Rate (kbps)
In Situ Science Package			
Vector Magnetometer (with boom cables)	0.8	0.5	1.2
Solar Wind Ion Composition and Electron Spectrometer (with mass allowance for implementing nadir viewing)	4.4	4.4	15.6
Energetic Particle Composition Spectrometer	0.7	0.6	4.8
Plasma Wave Sensor (with boom cables)	2.5	2.5	9.6
Fast Solar Wind Ion Detector	1.0	1.5	19.2
Data Interface Unit for *in situ* science instruments	0.3	0.8	—
Remote Sensing Package			
Visible Magnetograph–Helioseismograph	3.0	1.2	30
XUV Imager	3.0	1.2	30
All-Sky, 3-Dimensional Coronagraph Imager	2.8	2.0	2
Data Interface Unit for Remote Sensing Instruments	0.3	0.8	—
TOTAL	18.8	15.5	112.4

*Allocations for the two data processing units are not included.

The large-scale solar magnetic field at 4 R_S is expected to be on the order of 0.1 G. However, considering the dynamic nature of the corona, the vector magnetometer ought to be able to measure magnetic fields as great ~0.6 G to provide margin and accommodate the unexpected. In addition, the magnetometer must sense perturbations as small as 10^{-6} G to fully characterize the power spectrum of waves and fluctuations out to a radial distance of ~30 R_S. Finally, the high speed of the spacecraft at perihelion (~300 km/s) and the need to analyze thin structures imply a minimum sample rate of at least 10 vectors per second (i.e., ~1 measurement per 30 km), making the option for "burst" sample rates of ~100 vectors per second highly desirable.

Vector magnetometers that have been used in the exploration of the heliosphere and characterization of planetary magnetic fields (e.g., on Voyager, Galileo, Ulysses, Mars Global Surveyor, and Cassini) are well suited to the Solar Probe magnetic field measurement requirements. Furthermore, advances in sensor and electronics technology should allow these requirements to be met with a total instrument mass and power under 1 kg and 1 W, respectively. Therefore, the vector magnetometer is allocated 0.8 kg and 0.5 W in the Solar Probe strawman payload (including all analog and digital electronics and sensor cables). A triggered burst memory, shared and coordinated with the fast plasma and plasma wave analyzers, is highly desirable for characterizing dynamic events.

Solar Wind Ion Composition and Electron Spectrometer. Observations over the past 6 years, in particular with Ulysses, have taught us that the composition of the solar wind plasma gives us the most direct information about the source region of the solar wind and its characteristics. We have been surprised by recent measurements of highly unusual compositions in the CMEs observed in the slow in-ecliptic wind at 1 AU (Gloeckler et al., 1999a), which give

clues to the complex mix of plasmas originating in both hot and cold regions of the corona and their evolution during transit from their source to 1 AU. Studies of the evolution of the solar wind over distances of several astronomical units suggest that the mapping back to the source region becomes increasingly uncertain with increasing distance. Even the best measurements of the solar wind at 1 AU will not give us the definitive answer on how the solar wind is formed.

Clearly, to understand solar wind acceleration and pinpoint the wind's source region, it is imperative to characterize the solar wind in, or as close as possible to, the regions where its acceleration takes place. To achieve this we must find, for example, the dependence on altitude of fundamental kinetic parameters (bulk speed, temperature, temperature anisotropy) and non-Maxwellian features for a number of ion species as well as for electrons. The velocity distributions of a number of key ions as well as electrons are therefore essential components of the Solar Probe measurement requirements to meet the first two category A science objectives.

Table 2 summarizes the measurement requirements for the Solar Wind Ion Composition and Electron Spectrometer. In addition to measuring the distribution functions of protons and electrons (from which key kinetic parameters can be derived), we should measure the distribution functions of the dominant charge states of He, C, O, Ne, Si, and Fe (for example), with a time resolution of ~10 s. Charge state spectra for these elements that relate to the temperature at freezing-in of ionitation should also be obtained. The energy range should be as wide as possible, at the low end to catch the slowest solar wind and at the high end to just overlap the low-energy limit of the Energetic Particle Composition Spectrometer. Near perihelion, Solar Probe's thermal shield obscures the trajectories of particles coming from the direction of the Sun. This "shadow" cuts into the bulk of possible measurements of the distribution function of ions. The effect is mitigated somewhat by the aberration of solar-wind flow, depending, in turn, on the wind bulk flow speed (cf., Section 5.4, Fields of View). However, aberration may not fully solve the problem. The Science Definition Team has agreed that nadir viewing and a wide field of view are essential for measurements of the complete velocity distributions, which are expected to be broad and complex in the solar wind acceleration region.

We anticipate that techniques now in use (e.g., electrostatic deflection, time-of-flight spectrometry, low energy threshold measurements, etc.) can be combined in a miniaturized instrument to achieve the measurement objectives listed in Table 2. Because the fluxes near the Sun are large, and because microelectronics advances continue to reduce mass and power requirements, it should be possible to provide a Solar Wind Spectrometer that includes a nadir-viewing deflector system meets all thermal constraints within the allocations of mass (4.4 kg) and power (4.4 W) listed in Table 3 (cf. Zurbuchen et al., 1998). With some onboard computations, a bit rate of 15.6 kbps should be adequate for achieving the required time resolution.

Energetic Particle Composition Spectrometer. Energetic particles can be used in two ways on Solar Probe. First, they can remotely probe the structure of the solar plasma and magnetic field because of their high mobility. Second, they will provide fundamentally improved information about the acceleration sites and processes on the Sun. Their energy and composition give valuable, unique information concerning the plasma and magnetic field in the regions where they are accelerated and in the regions through which they move to the point of observation. In this case, the energetic particle instrument may also be regarded as a remote-sensing detector.

Almost all of our information about energetic particles from the Sun comes from measurements at 1 AU. Data from the two Helios spacecraft that came as close as 0.3 AU to the Sun are the only exception. The solar particles interact with the interplanetary medium through which they have traveled and, consequently, the measurements are not a true reflection of the particle distributions and composition close to their origin. The basic unanswered questions of how these particles are accelerated and fractionated can be answered only by *in situ* measurements on a Solar Probe Mission.

Solar energetic particle events have been subdivided into two main classes. *Impulsive events* are enriched in heavy ions, most prominently in Fe, and most of the time also in ^{3}He. *Gradual events* resemble more

closely the photospheric composition, with some mass and ionization-potential-related bias (e.g., Reames, 1992, 1997; Reames et al., 1996). The acceleration in impulsive events is thought to occur in the flare site, with resonant wave absorption being responsible for the drastic ^{3}He enrichment. The gradual events are believed to be associated with CME-driven shocks that are effective up to much larger distances from the Sun. Close to the Sun, angular and energy distributions will be largely free of the interactions with the interplanetary medium. Measurements of the composition and angular and energy distributions of the particles from both types of events, along with magnetic field data, will thus provide the information necessary to determine the origin and mechanism of acceleration and fractionation.

The large particle fluxes close to the Sun will result in a substantial increase in sensitivity, in particular to small impulsive events. The increase in sensitivity is counterbalanced by the short time of data acquisition and the fact that large energetic particle events do not occur continuously. However, there is ample evidence that small solar flares, or "microflares," occur at a high rate (e.g., Lin et al., 1991; Biesecker et al., 1993). These events very likely produce energetic particle fluxes below the sensitivity level of instruments at 1 AU, but they should be detectable closer to the Sun. Also, during solar maximum, impulsive events occur on average at a rate of 2–3 per day on the solar disc (Reames et al., 1994). Since Solar Probe will pass perihelion twice, once during solar maximum and once during solar minimum, we expect to observe several impulsive events and a good sample of microflares at distances substantially smaller than 0.3 AU. The closer to the Sun that the events are observed, the more useful will be the observation data in separating interplanetary effects from local acceleration.

To study small solar energetic particle events adequately and to distinguish impulsive events, an Energetic Particle Composition Spectrometer must be able to measure the energy spectra and angular distributions of electrons and ions. In addition, the ion sensor must able to separate H, He, CNO, and Fe. Separation of ^{3}He and ^{4}He is highly desirable. Along the entire trajectory, particles with sufficient gyroradii will be easily detected behind the heat shield. The allocation of spacecraft resources in Table 3 is consistent with current developmental work (McNutt et al., 1996b).

Plasma Wave Sensor. The second and fourth category A science objectives require the characterization of magnetohydrodynamic and plasma turbulence that may induce plasma heating. Scintillation measurements made through the corona using both natural sources and spacecraft transponders have shown that turbulence in the corona is ubiquitous. However, the dynamical and energetic role of plasma waves in accelerating and heating the solar wind remain unknown. To detect MHD waves, other space missions have used magnetometers sampling the quasistatic magnetic field. The high field magnitudes and rest frame velocities predicted for the Solar Probe mission, however, mandate that a separate Plasma Wave System be used for these measurements. Electric field measurements (to detect electrostatic emissions associated with particle beams and shock-like structures) are also desirable.

One key functional element of the Plasma Wave Sensor is a triaxial search coil or triaxial loop with sufficient frequency and dynamic range to detect these waves. Three axes are vital to determine the wave modes involved through polarization analysis and determination of the direction of propagation. Nonlinear properties such as phase steepening and compression should also be detected. These data will allow investigators to derive both the resonant particle populations driving the associated instabilities and the resonant particle populations absorbing the wave energy. Frequencies can be driven into the kilohertz range by Doppler shift, and amplitudes can reach ~0.1 G (Moses et al., 1991). A search coil system will detect localized fast- and slow-mode shock waves that also can be Doppler-shifted to large frequencies. All of these objectives require a waveform capture system. Since wave compression and steepening has been shown to occur in waves at these frequencies relative to the ion-cyclotron frequency, compression and phase-steepening should be detected by a search coil/loop sensor. Both of these nonlinear effects strongly affect wave–particle interactions. To conserve data storage resources, the waveform data can be coupled to a low-data-rate spectrum

analyzer for continuous coverage, and it can operate in either a triggered or a prescheduled burst mode. Whistler waves that may be involved in electron and/or energetic ion thermalization will occur at higher frequencies.

A triaxial dipole antenna could be used to detect electrostatic emissions up to the plasma frequency (which will reach several megahertz at closest approach) and radio emissions beyond. A single-axis system should be adequate for spectral studies and crude waveform sampling, while multi-axis systems will enable polarization and direction-finding analyses, a capability especially interesting for bipolar pulse or radio burst studies. Again, a low-data-rate spectrum analyzer can be coupled with a high-data-rate, but intermittent, waveform-sampling capability. The length of the antenna elements is necessarily limited by the available area behind the Sun shield, thus reducing sensitivity. The anticipated large amplitudes (potentially up to 1 V/m) limit the need for sensitivity but require a large dynamic range. If the science required a larger antenna, however, studies have shown that the carbon–carbon material used in the thermal shield (see Section 4) has reasonably high conductivity and could be used for an antenna extending beyond the thermal shield.

Fast Solar Wind Ion Detector. If, as expected, plasma microphysics plays a fundamental role in the physics of the corona, then to adequately address the first, second, and fourth category A science objectives requires fast, but more limited, ion measurements in addition to the ion measurements from the plasma and particle spectrometers. One of the theories for coronal heating is the damping of the Alfvén/cyclotron waves in the solar corona. Such processes can occur on the time scale of the cyclotron period, which is ~400 Hz at 4 R_S. Extreme ion distribution functions have been inferred from SOHO/UVCS observations. If these inferences are correct, relaxation of this "free energy" in the form of wave generation and resonant wave–particle interactions will occur. Again, temporal scales are expected to be as fast as the proton/ion gyroperiods. Thus, to understand fully the physical processes of coronal ion heating and thermalization, measurements of the ion distributions coordinated with the Plasma Wave Sensor are required on gyrofrequency time scales.

In addition to techniques used in more comprehensive plasma spectrometers, new lightweight detectors capable of making 3-dimensional distribution function measurements on time scales of 10^{-2} s have recently been studied (Murphy et al., 1993; Randolph et al., 1998). These sensors use delta-doping of solid-state surfaces to reduce the dead layer of the material, allowing direct energy determination of incident low-energy solar wind particles. This technique eliminates the need for energy scanning and allows greatly simplified particle detection. The high fluxes near the Sun are particularly suitable for the small surface areas of these sensors. Other advances in pixelated solid-state devices could also be used advantageously for plasma-particle and imaging instruments. Active pixel sensing (APS) is a well-developed technology that allows individual pixel interrogation per readout at very low (milliwatt) power consumption. A combination of "sparse readout" capabilities (not all pixels are read out) and burst-mode operation can be used to achieve efficient use of downlink capacity.

The Remote Sensing Package:

The remote sensing package primarily contributes to the second and third Category A science objectives. This package identifies the source of energy that heats the corona. It provides data to construct the 3-dimensional magnetic and density structure of the corona that supplies the context for the *in situ* measurements as they are made.

Background for Imaging Requirements. High-resolution observations in the visible, EUV, and X-ray regions of the spectrum allow measurements of the fine structure of the magnetic field and the density structure of the corona that are fundamental to plasma and particle acceleration. Lower-resolution observations provide data on the state of the corona during the encounter and provide context for the particle and fields measurements. Low-resolution observations with large fields of view also allow tomographic reconstructions of the 3-dimensional structure of the corona. In the sections below the most critical measurements in different spectral regions are discussed. In particular, Solar Probe's trajectory allows views of the solar polar magnetic and density structures

that can be obtained in no other way, as well as spatial resolution not possible from Earth.

As a strawman disk-imaging design goal, the imaging resolution is about 20 km at 4 R_S. This areal resolution is more than an order of magnitude better than that of the largest future orbiting solar telescopes that have been seriously studied. (The highest spatial frequency passed by a 1-m telescope at λ5000 Å is 75 km.) Near the Earth, detection of 20-km structure corresponding to 0.028 arc-sec requires a 3.75-m telescope in the visible. Such a telescope is significantly larger than the Hubble Space Telescope. At 4 (20) R_S, a 5.1 (33) cm telescope is able to detect 20-km structures at λ5000 Å.

In the EUV (50–300 Å) and soft X-ray (1–20 Å) region of the spectrum, the minimum diameters required by diffraction theory for 20-km resolution are 22.4 (1.48) cm for 300 Å (20 Å) at the Earth. At these short wavelengths the optical quality required for diffraction-limited imaging cannot be achieved with any known polishing technique, although both EUV and X-ray mirrors can be polished to sufficient quality to achieve 2 arc-sec resolution. Such mirrors at 4 and 20 R_S can detect 20- and 128-km structures, respectively.

Most of the corona is optically thin, so that an imager will see the sum of all structures in the line of sight. Tomographic techniques can be applied to isolate individual coronal structures. For example, X-ray tomography has been attempted using time sequences of Yohkoh data. The results have been interesting, but because the Sun rotates at about 13°/day, the image reconstruction is confused by the evolution of coronal structures. Near closest approach, at 4 R_S, Solar Probe rotates its perspective of the Sun nearly a factor of 40 faster than solar rotation, which is enough to freeze a significant fraction of coronal features for tomographic studies.

Technical Implications of the Solar Probe Orbit for Disk Imaging. To understand the optical design that drives disk imaging, it is essential to understand the conditions imposed by an approximately parabolic orbit with closest approach at the solar equator. Table 4 contains properties for the case of 4-R_S closest approach. The Table has been constructed so that the resolution at 75° latitude approach is 75 km. This choice was made because the mean free path for photons in the mid-photosphere is between 50 and 100 km in the visible. Because Solar Probe approaches closer to the Sun as it nears the equator, this choice will allow scientists to investigate the continuum and optically thin structures with even higher resolution over most of the surface. A telescope with an angular resolution of 2.27 arc-sec is required.

Visible Magnetograph–Helioseismograph. The most critical measurements in the visible wavelengths are, in order of priority, the magnetic field, a proxy for the magnetic field, and the continuum intensity. Although measuring the full vector field is desirable, both measurement complexity and the data rate implications make such measurements extremely difficult. For the solar polar regions, the magnetic field is most likely to be clumped in isolated intergranular regions and oriented nearly vertically to the surface. Thus, Solar Probe instruments will be looking almost straight down on the fields, so that the longitudinal Zeeman components contain most of the information. To measure the longitudinal component of the magnetic field requires spectral isolation of a portion of a magnetically sensitive line as well as right- and left-circular polarization analyses. As one example, spectral isolation can be accomplished using a solid Fabry–Perot (F-P) interferometer, and polarization separation can be achieved with a polarizing beamsplitter and a quarterwave plate.

The high speed of the spacecraft along the orbital path presents two problems for an F-P measurement: motion blur and Doppler shift. The required exposure time for a magnetogram measurement is between 200 and 400 ms (from Table 4), so motion blur is a problem only near closest approach. In the polar regions, the spectral shift is most severe. During Solar Probe's inbound phase, the velocity component toward the Sun causes a blue shift of spectral lines. After closest approach, a similar motion away from the Sun causes a red shift.

To measure the longitudinal Zeeman effect, one wing of a Zeeman-sensitive line must be isolated. This requires a spectral bandpass of 0.1 Å. We consider FeI 6302 Å (Landé g = 2.5) as one example for magnetic measurements to illustrate our points. As

Table 4. Properties of mission with closest approach at 4 R_S, where θ is the polar orbit angle at the solar latitude shown. (θ = 0° when Solar Probe is at aphelion near Jupiter's orbit.)

Property	θ = 75 +75	θ = 90 +90	θ = 105 +75	θ = 120 + 60	θ = 135 + 45	θ = 150 +30	θ = 165 +15	θ = 180 +0
Distance (center of Sun to spacecraft, R_s)	10.8	8.0	6.36	5.33	4.69	4.29	4.07	4
Spatial resolution of telescope (km)	75.0	53.6	41.0	33.2	28.2	25.2	23.0	23.5
Velocity of spacecraft (km/s)	188.	218.	245.	267.	285.	298.	306.	309.
Time to cross equator (hours)	10.2	6.68	4.6	3.2	2.2	1.37	0.663	0
Velocity toward Sun (km/s)	149	154	149	134	109	77.2	40.0	0
Velocity of solar surface* (km/s)	10.6	19.3	30.6	43.4	56.2	67.2	74.6	77.2
Spacecraft rotation rate** (deg/hour)	3.14	5.72	9.06	12.9	16.7	19.9	22.1	22.9
Time to move pixel (s) (i.e., 1/2 resolution element)	3.54	1.39	0.671	0.382	0.251	0.187	0.158	0.149
Number of pixels in 15° interval	5811	7835	9940	11967	13731	15042	15742	—
Wavelength shift (Å at 6302 Å)	3.13	3.24	3.13	2.81	2.29	1.62	0.839	0
Tilt angle to compensate for wavelength shift. (degrees at 6302 Å)	2.71	2.76	2.71	2.57	2.32	1.95	1.4	0

* Calculated as the velocity of the point on the solar surface that is on the line connecting the center of the Sun and the spacecraft.

** Calculated as though Solar Probe always pointed along the Sun center line

the spacecraft encounters the Sun, the radial velocity component increases as the spacecraft approaches 90° solar latitude, and then decreases to zero at 0° latitude. From Table 4, the wavelength shift at 90° is 3.24 Å. When an F-P interferometer is tilted, it shifts its transmission peaks toward the blue in proportion to the square of the tilt angle. Assuming that the F-P is at the design wavelength of about 6300 Å at normal incidence and has a solid spacer with index 1.5, a tilt of 2.76° is required to shift 3.24 Å. (This assumes that magnetograms are made only on the inward portion of the encounter.) If tuning is accomplished mechanically, a range of 3° is probably sufficient to cover both the velocity shift and the temperature shift of the etalon, because of changes in the temperature of the experiment section of the spacecraft. An accuracy of 50 arc-sec (216 steps) is sufficient to set the wavelength to 0.05 Å. An electro-optically tuned F-P interferometer could also be used.

If a single F-P interferometer is used, it probably would have a free spectral range (FSR) of 2 Å (a finesse of 20), which is too narrow to be isolated with an interference filter. However, a pair of solid

etalons with thickness ratios of 3 to 4 would have an FSR of 8 Å. All etalons made of the same material have the same wavelength shift with angle. Therefore, the pair of etalons can be bonded together to form a single double etalon filter (DEF). DEFs were built during the development phase of the Hα telescopes for Skylab and worked very well. A 0.1-Å DEF could be effectively blocked by an all-deposited 5-Å thin-film interference filter. The blocker has a temperature sensitivity of about 0.2 Å/°C and will not require temperature control if the temperature of the spacecraft payload bay is controlled to ±5°C. If the temperature is not controlled to that level, temperature control or tilt adjustment can be used to compensate.

The proper wavelength setting can be determined by scanning the DEF through its full tuning range. This task is somewhat complicated because the spacecraft is moving rapidly across the solar surface. By adding all the pixels in the image together, however, it should be possible to make a mean spectral scan sufficient to establish the proper set point for the DEF. This technique has been used on the ground to set the wavelength of tunable filters. It is also used on the SOHO/MDI experiment to set the wavelength of the MDI 0.05-Å filter.

If spacecraft resource constraints prevent a direct magnetic measurement, images in the CH bandhead (~4300 Å), the G band, supply the next-best indicator of the magnetic field locations. The bandhead is sensitive to the local heating in the flux tubes, and thus the intensity is a proxy indicator of magnetic field. The clustering of these temperature-sensitive molecular lines near bandheads provides two advantages over a magnetograph: (a) a relatively lower-resolution filter can isolate this spectral feature, and (b) required exposure times are significantly less (see Section 3.3.2 of Axford et al., 1995). Unfortunately, when flux tubes exceed 300 km in diameter the CH bandhead no longer brightens, so that local increases in G-band intensity do not indicate all the magnetic field locations. However, nearly all of the small bright points in the G band are coincident with compact magnetic structures. Because the poles are far away from any active regions, it is reasonable to assume that virtually all of the magnetic field is in the form of small flux tubes, and, hence, that a G-band image is a good proxy indicator for the locations of magnetic field.

The best ground-based images in the G band show structures of 100 km. The corresponding magnetic features are always larger. There are several reasons for the difference in size, but the largest contribution to the size increase is "seeing blur." For Solar Probe, it would be extremely interesting to know the difference between the sizes of structures seen and, at the same time, to map the magnetic field. Well-exposed diffraction-limited G-band images can be made with a 12-Å filter in an exposure time of 10 ms. Thus a simple imaging system using a fast frame transfer device can make images without use of a shutter and without problems from image motion blur.

XUV Imager. Here XUV refers to the spectral region between 61 and 304 Å. From Table 4, we see that to achieve 20-km spatial resolution at the solar equator, a 2 arc-sec (0.315 arc-sec) angular resolution telescope is required (for these two wavelengths). If the telescope is diffraction limited, a diameter of 0.314 cm will suffice. In the XUV, the regions emitting light are optically thin, so in principle, arbitrarily fine structures can be observed. The desired measurements are the topology, density, temperature, and velocity of the coronal structures. In the XUV, only fleeting rocket flights have captured images of 1 arc-sec quality. The Transition Region and Coronal Explorer (TRACE) produces time sequences with 1 arc-sec resolution. These data reveal that most of the coronal structures are at or below the resolution of TRACE, strongly suggesting that there is much fine structure in the corona. Very high resolution observations of the transition region and coronal structures are a high priority for meeting Solar Probe's second category A science objective.

All-Sky, 3-Dimensional Coronagraph Imager. The all-sky coronagraph imager on Solar Probe will image the ambient and surrounding corona in white light. The extended structure of the white-light corona is visible from the ground only during solar eclipses. In space, an artificial eclipse can be produced with techniques implemented on several orbiting coronagraphs. Rejecting the solar radiation makes the white-light corona readily accessible. The white-light corona is generated from Thomson

scattering of photospheric radiation by ambient unbound coronal electrons. After appropriately accounting for geometrical factors and the variation of the ambient solar radiation along the line of sight, the image of the white-light corona reflects the integral of the electron density along the line of sight. These factors cause the line-of-sight integral to be heavily weighted toward electrons along the plane of the sky. Panoramic images of the solar corona are available from SOHO/LASCO (Brueckner et al, 1998). These white-light images, in combination with the XUV images, permit study of the solar corona from the edge of the solar disk to 32 R_S. The SOHO images clearly show that the corona is rooted in the global structures of the solar magnetic field and that material is being continuously injected from the underlying solar structures.

Deriving the 3-dimensional structure of the streamer belt from single-viewpoint, white-light coronagraph images has proven to be a difficult task. With the assumption of a static corona, solar rotation can be used to provide different viewpoints. However, the coronal density distribution is undergoing continuous change, which gives rise to substantial uncertainty in these reconstructions. A comprehensive field-of-view white-light coronagraph onboard Solar Probe could provide images of the solar corona from many different viewpoints along the trajectory within a relatively short time. For example, the polar trajectory of the satellite will permit the longitudinal structure of the streamer belt to be directly observed simultaneously in its entirety for the first time. Such a reconstruction is critically important in establishing the context for measurements made by the onboard particle instruments.

An all-sky imager with 1° resolution and a photometric accuracy of 0.5% with images taken every few degrees will allow a high-quality density reconstruction to be obtained. Due to the large variation in the scene brightness, the detector must have a dynamic range of >1000. Depending on the detailed design, multiple exposures may be needed to provide high signal-to-noise coverage of the complete scene. To avoid blurring of the images due to spacecraft motion and other effects, the exposure times should be limited to less than 1 minute.

Additions to achieve secondary science objectives:

Enhancing the measurement capabilities of the strawman instruments to address some or all category B and C science objectives (in addition to category A science objectives) is highly desirable, but only without increases to required spacecraft resources (Table 3). For example, dust impacts on the Plasma Wave Sensor antennas provide impulsive signatures that can be interpreted to provide information on the impacting particles (e.g., Tsintikidis et al., 1995) (a category B objective). Another category B objective—establishing the relationship between plasma structures at the Sun and remote measurements from the Earth—follows naturally from a synthesis of Solar Probe measurements and measurements of opportunity made by satellites that are near the Earth during Solar Probe's perihelion passages. Finally, the spatial extent and compositional nature of the dust environment near the Sun (another category B objective) can be determined using measurements of extended inner source (EIS) pickup ions originating from atoms released from dust grains (Gloeckler and Geiss, 1998). The orbit of Solar Probe is ideal for probing the dust distribution near the Sun using these EIS pickup ions, which can be measured with the Solar Wind Ion Composition and Electron Spectrometer.

4. Reference Mission

(Note: Because the mission design is still evolving, sections 4–7 represent the mission status as of January 29, 1999.)

A unique feature of the Solar Probe spacecraft is the large but low-mass carbon–carbon parabolic heat shield to provide thermal protection for the payload and spacecraft. This heat shield also serves as the high-gain antenna (HGA) to provide a low-mass, compact spacecraft with high downlink capability. The shield has undergone extensive development and testing. In particular, tests of the carbon–carbon heat shield material show a mass loss rate far below the Solar Probe requirement that losses not contaminate the scientific measurements. Nadir viewing for the visible and XUV imagers is achieved by means of

carbon–carbon tubes that penetrate the heat shield and spacecraft bus to limit the solar flux reaching the detectors. In addition, the proposed baseline mission with two perihelion passes uses an advanced radioisotope power source (ARPS). An ARPS is currently defined as part of the baseline for each of the other two missions in the Outer Solar System/Solar Probe Program, Europa Orbiter and Pluto–Kuiper Express.

Solar Probe will be launched by a Delta III/Star 48 in February 2007 on a direct trajectory to Jupiter to minimize flight time (Figure 16). A Jupiter gravity assist places Solar Probe in a highly elliptical polar orbit around the Sun. Solar Probe's closest approach at 4 R_S takes place in late 2010, with the orbital plane perpendicular to the Solar Probe–Earth line (quadrature). This design permits dual use of the parabolic heat shield as the HGA. The first solar encounter takes place during a period of maximum solar activity, precluding observations of the less complicated Sun at solar minimum. Consequently, a second perihelion pass will take place early in 2015, at solar minimum. Again, closest approach is at 4 R_S, although forcing of the quadrature geometry is not yet guaranteed for the second pass.

For each of the two passes, encounter measurements by the *in situ* instruments start 10 days before closest approach and end 10 days after perihelion passage (Figure 17). During this 20-day period, the inner heliosphere (<~0.5 AU) and the corona will be observed *in situ,* at distances <~0.3 AU for the first time. Helioseismology observations begin 4 days (0.2 AU) before closest approach. The most intense observation by all instruments takes place in the 2-day period at distances of <20 R_S from the Sun. During this period, Solar Probe will make high-time-resolution, *in situ* measurements in the inner corona; high-spatial-resolution observations of the solar surface from pole to equator to pole; and 3-dimensional pictures of the solar corona as the spacecraft flies through it.

4.1. Mission Timeline

The reference Solar Probe mission starts with launch from the Eastern Test Range at Cape Canaveral, Florida, on February 15, 2007 on a Delta III launch vehicle augmented by a Star 48V upper stage. The interplanetary trajectory takes the spacecraft first to Jupiter, for a gravity assist, and then on to the Sun. The flight takes about 3.7 years to perihelion 1 and 8.1 years to perihelion 2. Figure 16 illustrates the interplanetary trajectory to the first perihelion. Table 5 summarizes the major events of the reference mission.

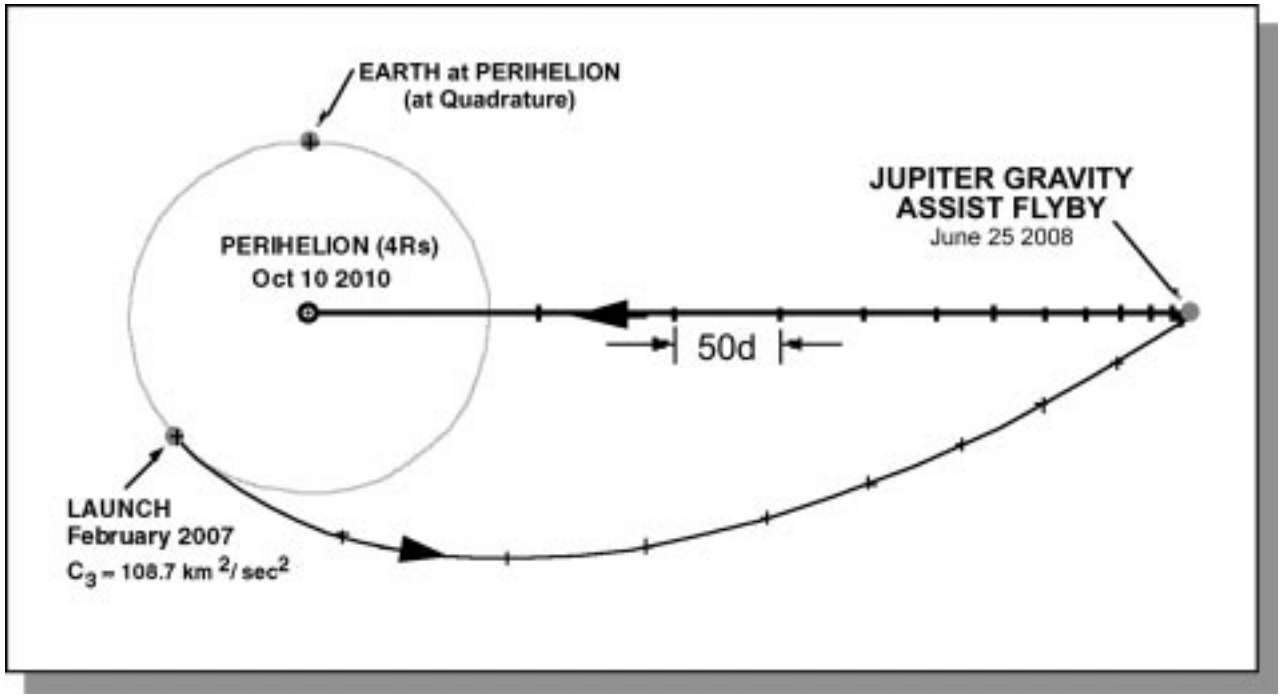

Figure 16. Interplanetary trajectory to perihelion 1.

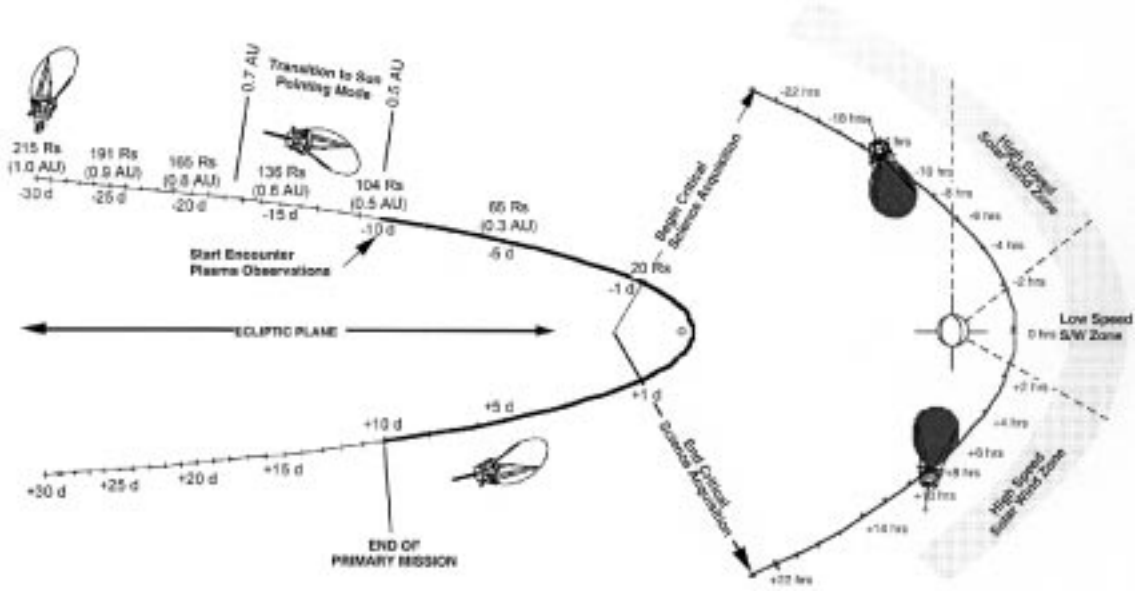

Figure 17. Perihelion 1 trajectory as seen from the Earth.

Table 5. Event summary for the reference Solar Probe mission, incorporating a Jupiter gravity assist (JGA).

PHASE	DESCRIPTION	EVENT MARKER
Launch	Launch (L) and interplanetary injection	15 Feb 2007
Cruise 1	Earth-to-Jupiter cruise	L + 30 days to JGA – 90 days
JGA	Jupiter gravity assist	25 Jun 2008
Cruise 2	Jupiter to perihelion 1 (P1) cruise	JGA + 74 days to P – 30 days
Start P1 primary mission	Begin primary science data acquisition for P1	P1 – 10 days (0.5 AU)
Critical science data acquisition	Critical science data acquisition for P1	P1 $\pm$ 1 day ($\pm$ 20 R_S) (Perihelion 1: 10 Oct 2010)
End P1 primary mission	End primary science data acquisition for P1	P1 + 10 days (0.5 AU)
Cruise 3	Cruise from P1 to P2	P1 + 30 days to P2 – 30 days
Start P2 primary mission	Begin primary science data acquisition for P2	P2 – 10 days (0.5 AU)
Critical science data acquisition	Critical science data acquisition for P2	P2 $\pm$ 1 day ($\pm$ 20 R_S) (Perihelion 2: 15 Jan 2015)
End P2 primary mission	End primary science data acquisition for P2	P2 + 10 days (0.5 AU)
EOM	End of mission	P2 + 30 days

The gravity assist flyby at Jupiter (10.5 Jovian radii (R_J), retrograde southern target) rotates the trajectory upward to a 90° ecliptic inclination and slows the heliospheric speed of the Solar Probe so that it falls back toward the Sun for the first of two perihelion encounters at 4 R_S. Quadrature geometry (90° Sun-spacecraft-Earth angle) exists at the first perihelion to allow real-time communications using the spacecraft antenna/shield configuration.

In situ and remote sensing observations of the corona and the Sun are planned. About 10 days prior to perihelion (0.5 AU), periodic high-rate (~50 kbps), real-time telemetry begins. Plasma observations begin 10 days prior to perihelion and continue through to perihelion plus 10 days. Remote sensing observations (imaging) to investigate helioseismology begin when the spacecraft reaches 30° latitude and continue until perihelion plus 4 days (60 R_S). The end of the primary observation phase for each of the two perihelia occurs about 10 days past perihelion.

During the first perihelion pass, a part of the science data is transmitted in real time, and high-priority data also are stored on board. The stored science data are played back after the end of the critical data acquisition period (Figure 17). For the second perihelion pass, a real-time link will be evaluated later in the project life cycle.

4.2. Solar Probe Encounter Geometry

The Solar Probe trajectory uses a northern approach to the Sun, reaching a speed in excess of 300 km/s at perihelion. This results in a pole-to-pole passage of approximately 14 hours.

As noted in Section 4.1, the time of the first perihelion is chosen to allow quadrature geometry that assures a high-rate data link to Earth through the dual-purpose thermal shield/HGA of the spacecraft. Images of the Sun as seen from the spacecraft at various times during approach for a field of view (FOV) of 30° are illustrated in Figure 18. The location of the Earth relative to the trajectory allows Earth viewing of the perihelion longitude just prior to spacecraft overflight.

Because the thermal shield/HGA is fixed, there is a period during the incoming trajectory to perihelion 1 (P1) when it cannot point toward Earth and still maintain the necessary shield pointing for thermal control. This period is expected to occur from P1 minus 10 to P1 minus 6 days. During this interval, when real-time downlink to Earth cannot take place, data will be recorded. The data will be replayed after perihelion minus 6 days but before the perihelion pass.

In the reference mission design, quadrature conditions are not enforced for perihelion 2. However, quadrature during the second perihelion pass will be evaluated later in the project life cycle.

5. Spacecraft System Design and Payload Interface Constraints

5.1. System Overview

The flight system for the reference mission consists of a spacecraft bus that houses the engineering and science electronic subsystems (avionics and bus-mounted instruments), heat shield/HGA subsystem, ARPS, propulsion subsystem, aft instrument boom, and the kick-stage rocket motor. Several views of the spacecraft are shown in Figure 19. Figure 20 is a functional block diagram showing the major hardware elements.

Integrating the science payload into the engineering system is a key challenge for Solar Probe. Special consideration must be given to the thermal constraints and communication requirements in order to allow maximum science return for minimum mass and power. To achieve this, an integrated team will need to determine how functional elements should be distributed the between the science payload and the engineering system. Concurrent engineering and teamwork within the project will be required to ensure that the science objectives are met within the resource constraints of the mission.

5.2. Thermal

The thermal shield/HGA subsystem is the basis for the thermal control, operability, and survival of Solar Probe in the near-Sun environment. With the

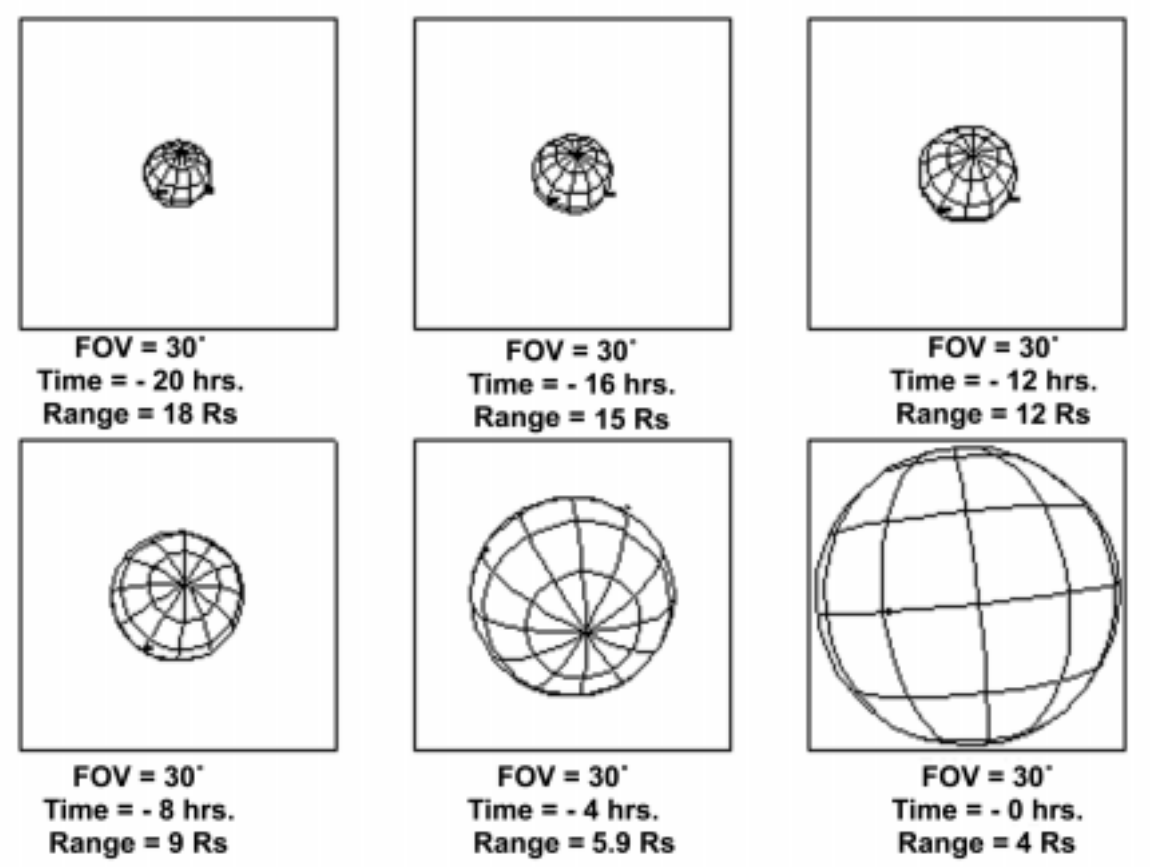

Figure 18. Typical incoming approach perspective.

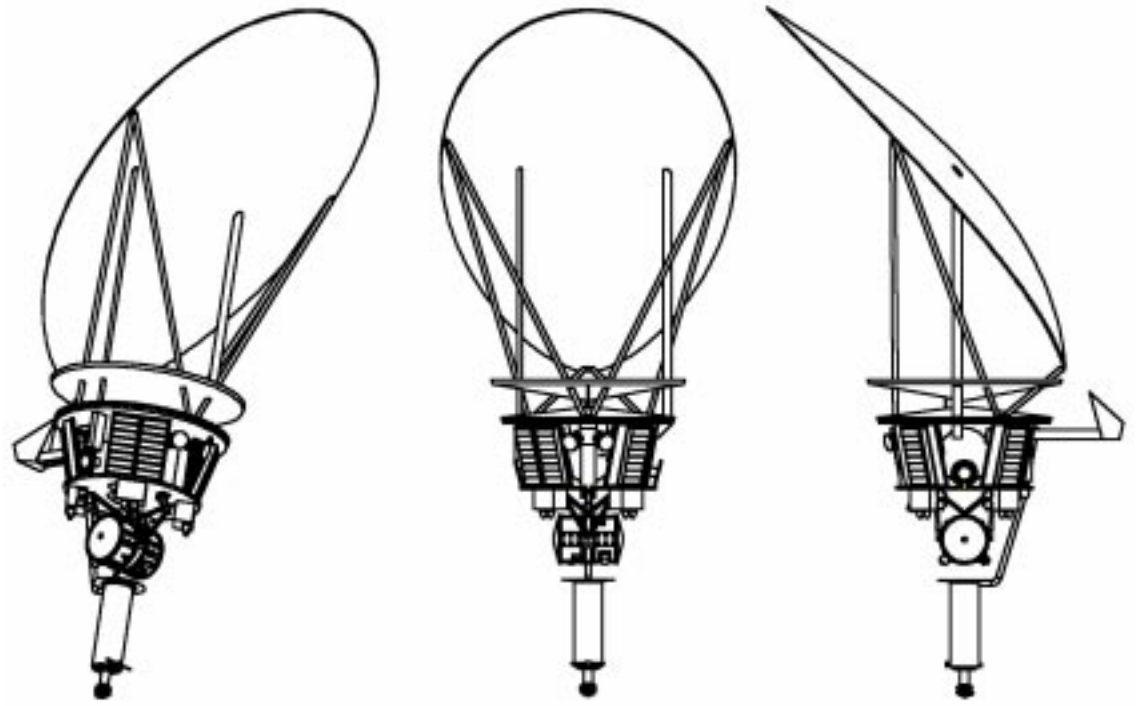

Figure 19. The Solar Probe spacecraft.

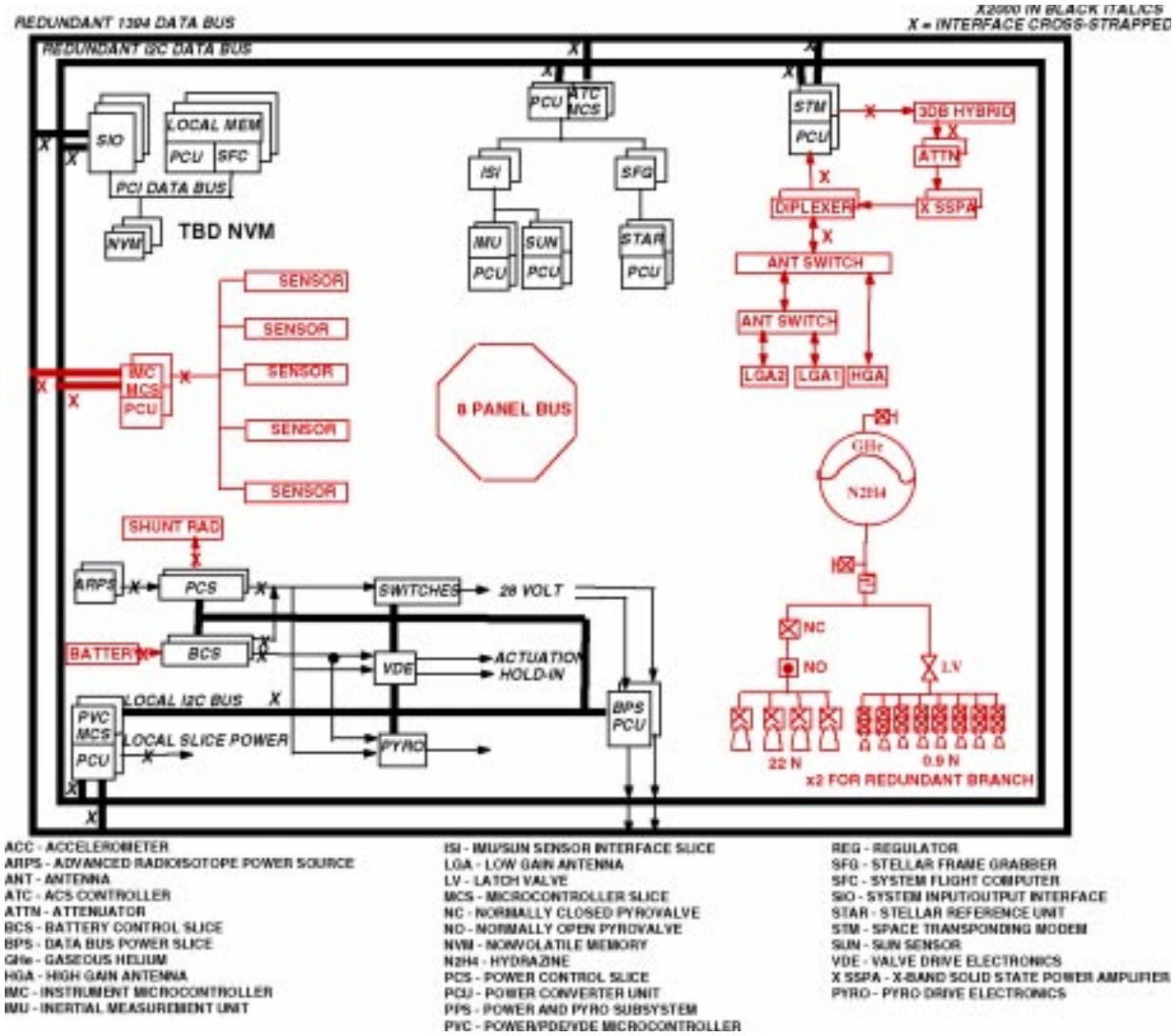

Figure 20. Functional block diagram of the Solar Probe.

current thermal design, the spacecraft bus components can operate within reasonable temperature ranges independent of distance to the Sun.

The spacecraft thermal design is capable of maintaining the propulsion system within a +5°C to +50°C temperature range and the bus within a –20°C to +50°C temperature range throughout the mission. The reference mission has distance extremes from 0.02 AU (4 R_S) to 5 AU (Jupiter orbit).

All instrument hardware located internally to the spacecraft bus must be able to withstand a flight operating and nonoperating temperature range of −20°C to +50°C. The maximum thermal dissipation for each bay in the bus allocated to science instruments is 28 W. This maximum thermal dissipation includes all solar heat absorbed by the instrument directly or through the light baffles in the HGA, in addition to the electrical power thermal dissipation. For the aft instrument boom, the maximum power dissipation is limited to the maximum heat that the instrument can radiate to space.

Thermal dissipation from the ARPS (which can provide about 197 W at end of mission) may be utilized to heat the bus if additional heat is required. The spacecraft may use radioisotope heater units (RHUs), electrical heaters, louvers, radiators, and thermal blankets for temperature control, as well as using ARPS waste heat.

5.3. Command, Control, and Data

The spacecraft data system is being developed by the X-2000 Program. It centers on two system flight computers (SFCs). These computers share engineering tasks and science tasks. A generic microcontroller serves as the standard interface between the data buses and remote terminals such as instruments. Each microcontroller provides interfaces to the four data buses: prime high speed, backup high speed, prime low speed, and backup low speed. The spacecraft data system will include a data storage capacity of ~6 Gbits to store all of the software and data for the mission. About 4 Gbits should be available for science data storage. The current baseline design employs nonvolatile flash memory (NVM). The planned software operating system for the spacecraft is VxWorks. The planned programming language is C^{++}.

5.4. Fields of View

The FOV for the bus-mounted instruments is 85° half angle on the tapered wedge or bay surface, as shown in Figure 21. This FOV surface is good for both sensors and radiators. In addition, an FOV for a nadir-viewing plasma spectrometer is shown. A ±20° FOV is shown for an instrument of this type having its own primary shield mounted on a side boom. For the aft instrument boom, the maximum FOV from the tip of the boom at the fully extended position is 340°. For the fully stowed position, the FOV is 322°.

5.5. Coordinate System, Mechanical Design, and Temperature Control

The spacecraft coordinate system is as shown in Figure 22. The spacecraft *Z*-axis is through the centerline of the spacecraft, with +*Z* in the thrust direction. (At perihelion, –*Z* points at the Sun.) The *X*–*Y* plane intersects the *Z*-axis at the base of the bus and is oriented with +*X* in the direction of the HGA boresight beam and with +*Y* in the direction of the spacecraft velocity vector at perihelion.

The HGA serves as the primary heat shield. Conical secondary shields exist between the primary shield and the bus. All of the shields are made of various types of carbon–carbon. The HGA dish and

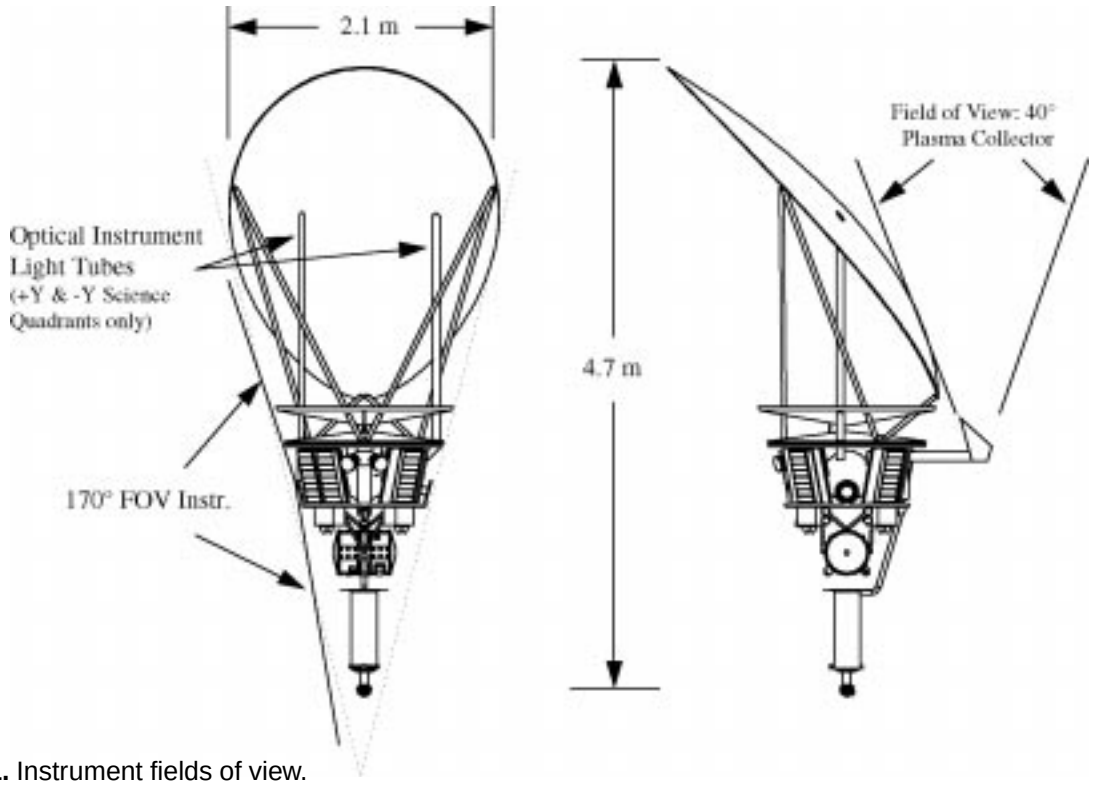

Figure 21. Instrument fields of view.

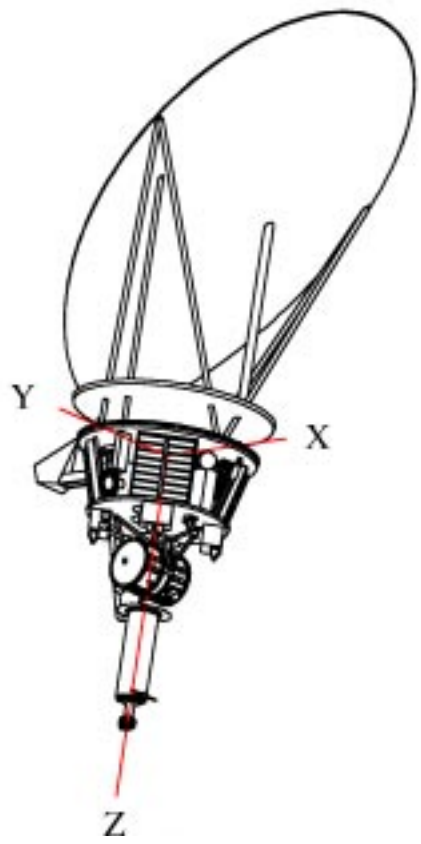

Figure 22. Spacecraft coordinate system.

secondary thermal shields make up the thermal shield/HGA system. The unusual shape and orientation of the off-axis HGA is consistent with the quadrature geometry at perihelion; quadrature allows a real-time communications downlinks with Earth at perihelion. Included in the thermal shield/HGA system are two light baffles. The light baffles, made of carbon–carbon, allow solar light to be attenuated as it passes through to the instruments that are maintained at room temperature inside the bus.

Below the HGA is the bus consisting of eight bays. Four of these are called bus panels and house the spacecraft avionics. Between the four panels are four tapered bays or wedges. Three of the tapered wedges (the $-X$, $+Y$, and $-Y$ bays) are for science use, and the fourth houses the attitude control sensors. Instrument interface attachments will be determined after the instruments are chosen.

Mounted in the center of the bus is the propulsion tank. The reference propulsion system is a single-tank monopropellant system utilizing hydrazine. The tank is structurally mounted to the bus closeout plate and located inside the bus structure. The closeout plate houses all of the propulsion components including the four thruster clusters. The closeout plate also has the integrated science payload boom attachment and the ARPS attachment bracket.

The aft instrument boom is stowed at launch and immediately deployed using a one-time actuator that moves the boom from a launch position to the flight position. The boom extension actuator is located on the boom. The instruments on the boom are located very close to the ARPS, which produces radiation (gamma and neutron) and a significant magnetic field. The instruments are also located in an area that may have some minor thruster-plume impingement from the *Z*-axis thrusters. This impingement is not a thermal issue but is a contamination issue. The disc shade below the ARPS helps reduce contamination.

5.6. Attitude Control

The Solar Probe spacecraft is 3-axis stabilized. Attitude is determined using star trackers, gyros, and Sun sensors. Each of these sensors is block redundant. Gyros are part of an inertial reference unit. Attitude control and ΔV maneuvers are accomplished by firing the 0.9-N thrusters located on the four thruster clusters.

Additional functions of the spacecraft attitude control system are to navigate and control the injection kick motor. Roll control during injection must be provided by the spacecraft.

Nearly continuous attitude estimation is planned. The star tracker must provide 4π steradian attitude determination. The gyros are used during maneuvers, and both trackers and gyros may be used for attitude reference during the perihelion passage. The Sun sensor is used principally for attitude acquisition during cruise and faults. Key baseline capabilities for the overall attitude control system are

Pointing accuracy	7 mrad
Pointing knowledge	3 mrad
Pointing stability	1 mrad/s

5.7. Telecommunications

The telecommunications system for Solar Probe reference mission consists of a parabolic HGA, block-redundant 3-W RF X-band solid-state power amplifiers (SSPAs) and block-redundant small deep-space transponders (SDSTs). A top-level diagram showing the telecommunications system architecture is shown in Figure 23. The telecommunications configuration shown is a unified uplink/downlink X-band design such that all telecommunications link functions can be utilized simultaneously—command, telemetry, Doppler tracking, and ranging.

The real-time telemetry rate near perihelion varies according to representative data shown in Figure 24. An additional fundamental assumption is that the amplitude scintillations caused by coronal perturbations on the downlink are infrequent transient events and are not expected to significantly affect this telemetry rate performance (see Bokulic and Moore, 1999).

5.8. Propulsion

The propulsion system provides the required onboard incremental changes in velocity and reaction attitude control capability for the spacecraft over the lifetime of the mission. The total propulsion ΔV is baselined at 90 m/s; it is sized for the Jupiter gravity assist trajectory reference mission with two 4-R_S flybys of the Sun. The system is a monopropellant system utilizing hydrazine. The thrusting system consists of eight 0.9-N thrusters, which are used both for propulsion and for attitude control.

6. In-Flight and Near-Sun Environmental Hazards

Generally recognized environmental hazards for Solar Probe fall into three categories:

1. Dust hazards
2. The radiation environment

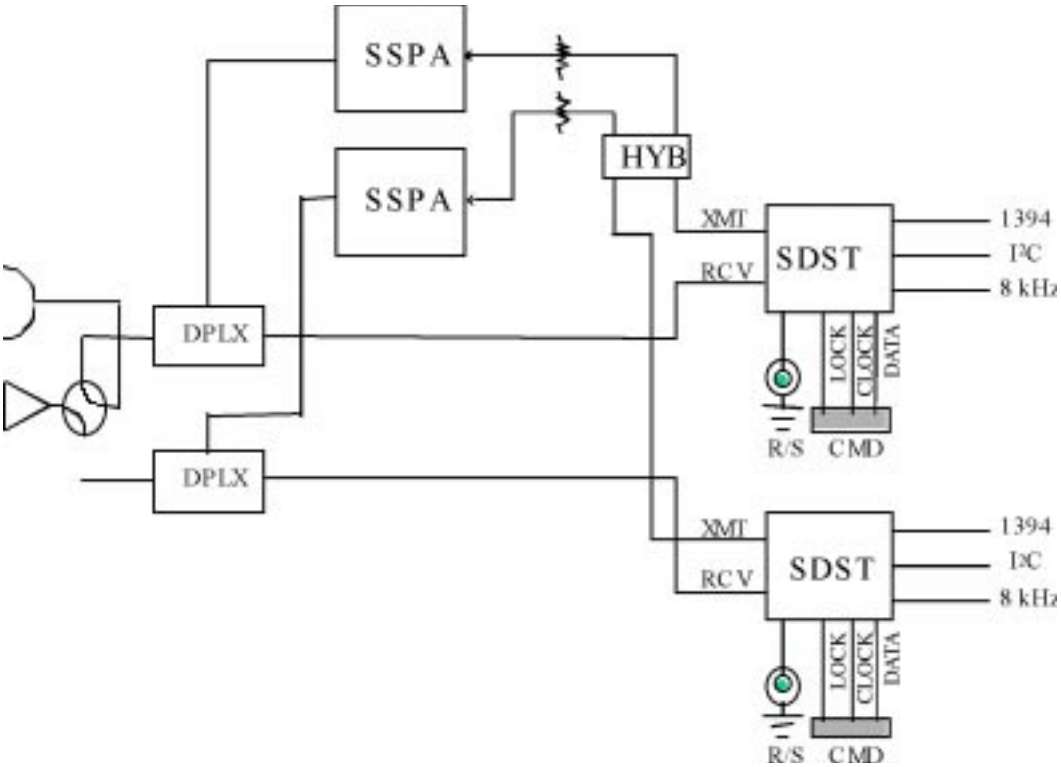

Figure 23. Telecommunications subsystem architecture. (CMD = command; DPLX = diplexer; HYB = hybrid device; R/S = Reed–Solomon coder; RCV = Receive; SSPA = solid-state power amplifier; SDST = small deep-space transponder; XMT = transmit.)

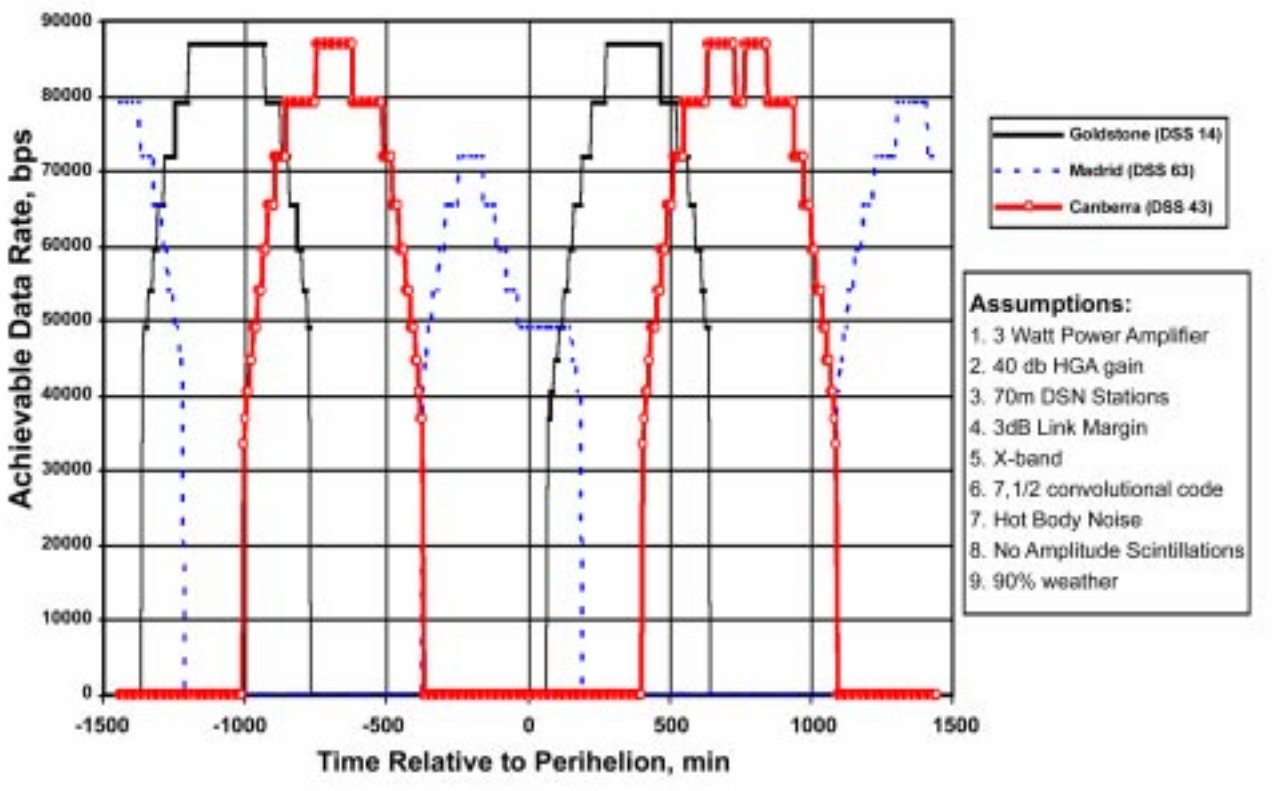

Figure 24. Solar Probe telemetry rate near perihelion on October 10, 2010.

3. Sublimation from the carbon–carbon thermal shield/antenna

Dust impact and radiation hazards are functions of the ambient (natural) environment. An additional source of radiation is the ARPS. The hazard of sublimation from the spacecraft's thermal shield is self-induced. The levels of all three natural hazards, as well as necessary mitigation levels and procedures, have been subjects of ongoing debate since the Solar Probe mission was first proposed in the late 1970s. The earliest work was done in conjunction with the Starprobe mission, an early version of Solar Probe (Neugebauer et al., 1978, on radiation; Goldstein et al., 1980, on outgassing and spacecraft potential). The most recent comprehensive work was completed at the Solar Probe Environment Workshop (Vaisberg and Tsurutani, 1995).

The three environmental hazards just listed can be further grouped in order of increasing problem levels:

1. *Measurement Contamination*—including obscuration of optics and detection of spacecraft-generated signatures of the *in situ* measurements
2. *Measurement Obscuration*—measurements dominated by the hazard environment, including both spacecraft-generated signatures and processing and detection failures in electronics caused by an increased radiation background
3. *Instrument Failure*—e.g., arcing, structural damage from grain impacts, permanent electronics failure from radiation damage
4. *Spacecraft Failure*—Structural, thermal control, and/or avionics failure producing the loss of the spacecraft and the mission

The maximum acceptable hazard level is just prior to encountering level (2); that is, contamination of measurements is classified as acceptable, although this implies that the contamination can be recognized and worked around or calibrated out.

6.1. Dust Hazards

There are no design-quality data on the magnitude of the dust environment near to the Sun. Observations of scattered light (the F-corona) suggest the

presence of dust near the Sun but yield no information on the size distribution, and there is ambiguity in separating thermal from scattering effects in the measured light intensities (Mann and MacQueen, 1995). Within 0.3 AU of the Sun, heating and sublimation of dust is expected to lead to a depletion in the dust environment (dust originates from a variety of sources and is decelerated on Keplerian orbits by the Poynting–Robertson effect) (Mann, 1995). Observations of zodiacal light from the Helios spacecraft suggest that a conservative extrapolation can be made using distance from the Sun $r^{-1.3}$ dependence, where most of the dust is concentrated toward the plane of the ecliptic and has an exponential scale-height distribution (Tsurutani and Randolph, 1990; Skalsky and Andreev, 1995). Extrapolations based upon this model suggest a worst-case mass flux in ~micron-sized particles of 10^{-9} g m^{-2} s^{-1} at 4 R_S. A random hit at typical expected speeds of $\gtrsim$200 km s^{-1} could cause structural failure of the spacecraft.

6.2. The Radiation Environment

The principal sources of radiation are Jupiter's radiation environment, the near-Sun radiation environment, potential solar flares, cosmic radiation, and the ARPS.

The ARPS environment assumes the use of an advanced radioisotope power source (ARPS) with eight general-purpose heat source modules repackaged from a spare Cassini radioisotope thermoelectric generator. The actual radiation exposure of an instrument assembly depends upon its configuration on the spacecraft and will require a radiation transport analysis.

The Solar Probe mission is subject to natural radiation hazards from the magnetospheric environment of Jupiter and from the solar coronal environment itself. A Jupiter flyby is required for any Solar Probe mission using present-day launch vehicles. Launch dates over the next two decades require a Jupiter flyby to within 10 R_J of the planet. This region has been well explored by the Pioneer 10 and 11, Voyager 1 and 2, and Ulysses spacecraft.

For a ~10-R_J flyby distance, the expected radiation environment at Jupiter is ~35 krad with 100 mil of aluminum shielding. By using approved parts lists and introducing functional redundancy of appropriate subsystems, this level of radiation background is easily dealt with. The same is true for single-event effects produced by galactic cosmic rays and/or solar proton events (Garrett, 1996).

The radiation hazard from the Sun itself remains unknown. Both shock acceleration and direct (flare) acceleration have been implicated in producing particles seen in the 10–100 MeV energy range. Work by Tsurutani and Lin (1985) and Reames (1995) suggests that the dominant component of the proton flux at 1 AU is due to shock acceleration. Such shocks occur ahead of fast CMEs, which occur primarily during solar maximum. Ulysses has indicated that CME-driven shocks can exist at high heliolatitudes (Gosling et al., 1994), with significant particle acceleration occurring. Wu et al. (1995) report that CME-related shocks first form at a substantial distance from the Sun (typically 15–20 R_S). In addition, since high-Mach-number shocks are more effective at accelerating energetic particles, the near-solar particle fluences would be less than an inward scaling of r^{-2} (fluence) or r^{-3} flux (Feynman et al., 1995).

Solar Probe approaches the Sun from high latitudes and passes over the near-equatorial active regions relatively quickly at perihelion. Both parts of this trajectory are good for minimizing the particle flux/fluence caused by solar events. Kiplinger and Tsurutani (1995) have examined the probability of a flare occurring when Solar Probe is within ±30° of the solar equator. Using the statistics of Reames (1995), they find the probability to be about 2% during solar maximum. Clearly, the solar flare fluence/flux at high latitudes needs to be studied more closely to better understand the quantitative doses.

6.3. Outgassing–Sublimation Hazards

Outgassing and sublimation can pose hazards to the Solar Probe in several ways. The most important likely problem is that neutrals released from the high-temperature heat shield will become ionized close enough to the spacecraft either to alter the properties of the solar wind ions and electrons or to

generate plasma waves that might mask observation of ambient plasma waves. An additional issue is contamination of spacecraft surfaces by deposition of neutral carbon. If the density of the neutral carbon gas is sufficiently low that the flow of carbon neutrals is collisionless, the problem does not appear to be a major one, because sensitive surfaces can be protected by restricting the line-of-sight to the hot neutral source. Proper prelaunch heat treatment can reduce the risk from outgassing, but sublimation remains as an unavoidable minimum. Sublimation rates are discussed in the following two sections. These sections discuss the ion pickup process and estimated mass loss rates and show them to be low enough to prevent interference with the science observations.

Sublimation rates:

In the design of the thermal shield, the following logic was used: (1) Sublimation of shield material (carbon) could interfere with measurements of the *in situ* environment. Such measurements are the rationale for the mission. (2) Shield sublimation is a function of the shield temperature and the thermal/optical material properties of the shield. (3) Shield temperature must be driven by the "acceptable" outgassing/sublimation/ablation rate—as determined by another calculation. (4) Shield temperature is then determined by the amount of solar loading versus the amount of radiative area. The actual calculations of shield temperature include both radiation and conduction (which is much less important). For the planned Solar Probe heat shield/antenna, a hot region near the tip of the shield dominates outgassing. Measured sublimation rates have been available from graphite for some time (Drowart et al., 1959). Preliminary indications (Valentine et al., 1997) are that outgassing from various carbon–carbon matrices is about an order of magnitude less than graphite, presumably due to surface energy effects.

The tip of the carbon–carbon heat shield is estimated to have an effective area of 0.4 m^2 at ~2250 K and 0.6 m^2 at ~2200 K. These areas supply most of the sublimation that is strongly temperature dependent. For materials fabricated using the chemical vapor injection technique, the loss rates are 0.0046 mg m^{-2} s^{-1} at 2242 K and 0.0015 mg m^{-2} s^{-1} at 2204 K. Since mass spectrometry data were not available in the Valentine et al. (1997) study, the JANAF thermochemical tables were used to estimate the relative amounts of loss of various multiatomic carbon neutral species (C_1, C_2, C_3, C_4, and C_5). If the Valentine et al. (1997) study results are used, the total mass loss rate for the current Solar Probe design is estimated to be about 3.3 10^{-3} mg/s; using the JANAF tables produces results that are about 5 times greater (1.6×10^{-2} mg/s). Note that this is the maximum sublimation rate that occurs at 4 R_S. When the spacecraft is further from the Sun, the temperature decrease leads to orders of magnitude less sublimation.

Mass loss rate and interference with science objectives:

Early in the Solar Probe concept studies, it was recognized that the composition of the thermal shield would drive how closely the spacecraft could approach the Sun before the *in situ* measurements would be corrupted. Goldstein et al. (1980) noted that the driving criterion was "a requirement of no important interference with scientific objectives." In particular, these authors were concerned to keep the effect on plasma wave and electron observations at a minimum. Positive ions can presumably be separated from *in situ* ions in the plasma measurements on the basis of ionization state and composition. However, sufficiently large mass loss rates could alter the local electric field near the spacecraft, adversely affecting plasma, especially electron measurements. Based upon the criterion that the spacecraft float to no more than 20 V with respect to the local plasma (and introducing a safety factor of 5), they derived a maximum acceptable outgassing rate of 3.0 mg s^{-1} for the entire shield system. An independent constraint based upon less than a 1% chance of an electron collision with sublimating carbon was an order of magnitude less stringent. Plasma wave and wake effects were found to be unimportant at this outgassing/sublimation level. The recent carbon–carbon material test showed sublimation rates far below this value (Valentine et al., 1997).

The question of pickup ion effects was investigated by Okada et al. (19/95), Goldstein (1995), and Tsurutani et al. (1995). Goldstein looked at the possibility that the pickup plasma would interact with the solar wind plasma via waves that stand in the

spacecraft frame. On this basis, the waves of interest are lower hybrid waves and electron-cyclotron waves. From the wave impedance for these types of waves, Goldstein (1995) estimated that a mass loss rate of 2.1×10^{-2} g/s would result in a maximum potential perturbation in the plasma of about 5 V. Because of uncertainties in the method of calculation, however, he recommended that the mass loss rate be limited to about 2×10^{-3} g/s. This work assumed a neutral ionization time of 30 s and a mass dominated by C_3 ions. Okada et al. (1995) examined the possibility that C_2^+ ions and related electrons might generate plasma instabilities. Using the Kyoto University Electromagnetic Particle Code (KEMPO), they found that no substantial waves were generated by either the ion or the electron pickup. The combined U.S.–Russian panel on Atmospheric and Electromagnetic Environment Group (Tsurutani et al., 1995) determined that the carbon/electron pickup process seems not to be a problem for Solar Probe.

The Science Definition Team obtained some simple checks on the work just described. As a check on the ionization rate assumed in the previous studies, W.-H. Ip independently calculated the ionization rates using more recent estimates of photoionization rates and electron impact rates. The results he obtained for photoionization and electron impact rates near the Sun are summarized in Table 6.

Note that for the results in Table 6, the C_1 and C_2 photoionization rates are from Huebner et al. (1992). The solar condition was assumed to be for the quiet Sun at solar minimum. No laboratory data exist for the photoionization cross sections of C_2 and C_3. The electron impact ionization rates for C_1 and C_2 were obtained from D. Shemansky (private communication, 1997). As with photoionization, the electron impact rate of C_3 is assumed to be the same as that of C_2. The electron temperature is assumed to be 10^6 K; case (a) is for electron number density of $10^4/cm^3$ and case (b) is for $5 \times 10^4/cm^3$.

The effect of mass loading upon directly decelerating the solar wind was found to be negligible. Within about 2 m of the spacecraft, the pickup ion number densities were found to be comparable to the solar wind proton densities, but this would not affect the observations. (Note that this conclusion is based on the old, higher outgassing estimates calculated from JANAF tables rather than on the lower estimates obtained from Valentine et al., 1997).

In view of these results, the most likely (if any) source of interference with the measurements would be generation of plasma waves by the pickup ions, thus confusing the interpretation of the waves normally present in the solar wind. It was assumed that the lower hybrid (modified two-stream) instability would be the most likely source of wave growth. This instability typically requires pickup ion density to be about 10% of the ambient ion density (at least if the instability is to be isolated in the frequency spectrum). For the case of encounter at 4 R_S, the maximum growth rate was taken as $0.5\omega_{LH}$, where ω_{LH} is the lower hybrid frequency, and the minimum growth length was taken as the solar wind velocity divided by this growth rate. On this basis, the minimum growth rate was found to be 120 m, and full growth to saturation is typically found only after $30/\omega_{LH}$. As the scale size of the ion cloud where the density is 10% or greater is much smaller than 120 m, it is concluded that the lower hybrid instability is not likely to be a cause of interference.

7. Mission Operations Concept

As with the Europa Orbiter and Pluto-Kuiper Express missions, Solar Probe has short critical observation and activity periods interspersed with relatively long cruise segments of low activity. For such long missions, appropriate trade-offs between autonomy, low-level monitoring, and high activity periods must be incorporated into mission operations

Table 6. Photoionization and electron impact rates at 4 solar radii.

	Photoionization	Electron impact	Total (Case a)	Total (Case b)
C_1	2.4×10^{-2} /s	1.34×10^{-3} /s	2.53×10^{-2} /s	3.07×10^{-2} /s
C_2	2.6×10^{-3} /s	2.38×10^{-3} /s	4.98×10^{-3} /s	1.45×10^{-2} /s
C_3	2.6×10^{-3} /s	2.38×10^{-3} /s	4.98×10^{-3} /s	1.45×10^{-2} /s

in order to assure mission success while controlling operational costs.

To greatly reduce the cost of mission operations during a long flight, the "beacon cruise" concept has been developed. The high- or medium-gain antenna points continuously toward the Earth during cruise, with the receiver operating and the transmitter broadcasting an uncoded carrier. The broadcast carrier has three possible tones: (1) everything's okay; (2) data are ready for downlink; or (3) a serious problem needs *immediate* attention.

The broadcast carrier can be received by smaller ground stations than are normally associated with deep-space missions, so that much of the spacecraft health monitoring can be done on a loosely scheduled basis by non-JPL partners (i.e., universities, industry, other NASA centers) or other non-DSN facilities. If the tone indicating a problem is received, then the spacecraft is tracked more intensively by the DSN, and an emergency response team is quickly assembled to resolve the problem.

The Solar Probe spacecraft will feature a large degree of autonomy, self-monitoring, self-commanding internal fault protection in both software and hardware, and automated onboard resource management, so that a small ground team will be needed during cruise. With the robust power and thermal control capabilities of a spacecraft powered by ARPS generators, the time criticality of recovery from possible anomalous spacecraft conditions during cruise is far less than for solar-array powered spacecraft. Some months before the solar encounters, a larger ground team will be assembled to perform the final instrument calibration, planning, and implementation of the science encounter phase of the mission.

The mission operations and data handling concept for the Solar Probe Project has been specifically designed to reduce operations cost while supporting the Solar Probe Science Team, promoting educational outreach, and reducing development costs. The main attributes of this mission operations and data handling concept are

- *Constrained Cruise*. Constrained operations during cruise assume limited contact with the spacecraft, infrequent science sensor status and performance checks, and limited encounter sequence verification tests. Science team activity will be minimal during this period.

- *"Canned" Encounter Sequence*. The Science Team will define a pre-programmed encounter sequence for automatic execution onboard, test it during prelaunch mission simulations, and refine and re-verify it during the long cruise. The encounter sequence for the second perihelion pass will be updated based on findings from the first pass.

- *A Long Mission*. The launch will be followed by a checkout and calibration phase lasting about 3 months. The spacecraft will fly in beacon cruise mode for about 1 year before reaching Jupiter. For the 5 weeks during the Jupiter gravity assist, DSN coverage will be increased to daily passes, and additional staff will be added to the operations team. After about 2 more years of beacon cruise operations, a solar pre-encounter phase will begin at perihelion minus 60 days.

- *First Solar Pass*. Starting at perihelion minus 30 days, continuous DSN coverage will allow science data to be continuously downlinked in real time at ~50 kbps (the real science downlink data rate after packet, frame, coding, and engineering data overhead have been accounted for). To accommodate occasional blackout periods and the possibility of ground station failures, science data may be redundantly recorded onboard and played back later.

- *Second Solar Pass.* After about 3.5 years of very low activity beacon cruise, the second pre-perihelion operations phase begins at perihelion minus 30 days.

- *A Unified Flight and Ground Data System*. Both flight and ground data systems are included in an integrated end-to-end mission operations system (EEMOS). This unified architecture enables functions to be tested first on the ground and then integrated into the onboard flight system. It enables trade-offs to be made between flight and ground autonomy, and it provides a conservative approach to the use and implementation of autonomy.

- *Automated Operations*. Autonomy, to lower the cost of mission operations, will include automated fault detection, isolation, and response for spacecraft and science sensor faults; the ability to autonomously initiate commands and sequences based on detected events or conditions; and the generation of a highly abstracted set of performance indicators for downlink to ground controllers.

- *Operations System Tools Available for Development*. Prototype versions of mission operations and data handling tools will be supplied to the Science Investigation Teams early in the development phase. These tools will support science sensor test and calibration, payload and spacecraft integration and test activities, and prelaunch mission simulations and rehearsals and will continue support throughout the mission. As the project matures through these phases, and as the Science Investigation Team members have a chance to use and evaluate these tools, the tool set will be progressively enhanced and expanded. This progressive implementation ensures that the tools are well tested before launch; that the Solar Probe mission operations system and data subsystem are specifically tailored and developed; and that these systems can evolve to meet the needs of users during the solar encounters.

- *Distributed Network of Users*. The end-to-end mission operations system architecture is distributed to include a network of remote workstations. Through this network, the distributed science team members will be able to access the full range of mission data and participate in mission operations activities from their home institutions.

- *Educational Emphasis*. The mission operations and data handling effort features and will continue to feature student participation, educational outreach, and public information. Throughout the mission, science and engineering data products and information will be made available to schools and to the public.

Cruise operations and data handling activities will be carried out by a group of JPL experts teamed with a university group. The university participation enables students to participate in this invaluable educational experience, while enabling significant cost reductions throughout the long mission.

8. References

Axford, W. I., et al., *Close Encounter with the Sun: Report of the Minimum Solar Mission Science Definition Team*, JPL D-12850, Jet Propulsion Laboratory, Pasadena, CA, 31 August 1995.

Biesecker, D. A., J. M. Ryan, and G. J. Fishman, in *Advances in Solar Physics, Lecture Notes in Physics*, G. Belvedere, M. Rodono, and G. M. Simnett, eds., *vol. 432*, p. 225, 1993.

Bokulic, R. S., and W. V. Moore, Near Earth Asteroid Rendezvous (NEAR) solar conjunction experiment, *J. Spacecraft Rockets*, *36*, 87–91, 1999.

Brueckner, G. E. , et al., Geomagnetic storms caused by coronal mass ejections (CMEs): March 1996 through June 1997, *Geophys. Res. Lett.*, *25*, 3019–3022, 1998.

Corti, G., et al., Physical parameters in plume and interplume regions from UVCS observations, in *The Corona and Solar Wind Near Minimum Activity*, ESA SP-404, 289–294, Noordwijk, 1997.

Drowart, J., R. P. Burns, G. DeMaria, and M. G. Inghram, Mass spectrometric study of carbon vapor, *J. Chem. Phys.*, *31*, 1131–1132, 1959.

Feldman, W., et al., *Solar Probe: Scientific Rationale and Mission Concept, A Report of the 1989 Solar Probe Science Study Team*, JPL D-6797, Jet Propulsion Laboratory, Pasadena, CA, November 1989.

Feynman, J., B. E. Goldstein, and G. C. Spitale, The radial dependence of solar proton fluences, in *Proc., First US–Russian Scientific Workshop on FIRE Environment*, IKI, Moscow, Russia, pp. 55–68, 1995 (JPL reorder no. 95-3).

Garrett, H., *Solar Probe Environments Mitigation Techniques*, presentation to Solar Probe Science Definition Team, 5 December 1996.

Geiss, J., et al., The southern high-speed stream: Results from the SWICS instrument on Ulysses, *Nature*, *268*, 1033–1036, 1996.

Gloeckler, G., and J. Geiss, Interstellar and inner source pickup ions observed with SWICS on Ulysses, *Space Sci. Rev.*, *86*, 127–159, 1998.

Gloeckler, G., L. A. Fisk, S. Hefti, et al., Unusual composition of the solar wind in the 2 May 1998 CME observed with SWICS on ACE, *Geophys. Res. Lett., 26*, 157–160, 1999a.

Gloeckler, G., S. T. Suess, S. R. Habbal, R. L. McNutt, J. E. Randolph, A. Title, and B. T. Tsurutani, Solar probe: A mission to the Sun and inner core of the heliosphere, *Proc. Toward Solar Max 2000, Yosemite 1998*, in press, 1999b.

Goldstein, B., Standing wave effects on electric potential of the outgassing cloud, in *Proc., First US–Russian Scientific Workshop on FIRE Environment*, IKI, Moscow, Russia, pp. 133–139, 1995 (JPL reorder no. 95-3).

Goldstein, B. E., W. C. Feldman, H. B. Garrett, I. Katz, L. Linson, K. W. Ogilvie, F. L. Scarf, and E. C. Whipple, *Spacecraft Mass Loss and Electric Potential Requirements for the Starprobe Mission*, JPL 715-100, Jet Propulsion Laboratory, Pasadena, CA, 1980.

Gosling, J. T., S. J. Bame, D. J. McComas, J. L. Phillips, B. E. Goldstein, and M. Neugebauer, The speeds of coronal mass ejections in the solar wind at mid heliographic latitudes, *Geophys. Res. Lett., 21*, 1109, 1994.

Grall, R. R., et al., Rapid acceleration of the polar solar wind, *Nature, 379*, 429, 1996.

Habbal, S. R., ed., *Robotic Exploration Close to the Sun: Scientific Basis*, A1P Conf. Proc. 385, Am. Inst. of Phys., Woodbury, NY, 1997.

Habbal, S. R., G. Gloeckler, R. L. McNutt, Jr., and B. T. Tsurutani, The solar probe mission: A search for the origin of the solar wind and an unprecedented view of the solar surface, *Proc. of "A Crossroads for European Solar & Heliospheric Physics, ESA SP-417*, Tenerife, Canary Islands, March 23–27, published June 1998.

Huebner, W. F., J. J. Keady, and S. P. Lyon, Solar photo rates for planetary atmospheres and atmospheric pollutants, *Astrophys. Space Sci., 195*, 1–294, 1992.

Kiplinger, A. L., and B. T. Tsurutani, Fire under fire: Proton probabilities at perihelion, in *Proc., First US–Russian Scientific Workshop on FIRE Environment*, IKI, Moscow, Russia, pp. 273–279, 1995 (JPL reorder no. 95-3).

Kohl, J., et al., First results from the SOHO Ultraviolet Coronagraph Spectrometer, *Sol. Phys., 175*, 613–644, 1997.

Li, J., et al., Physical structure of a coronal streamer in the closed field region observed from UVCS/SOHO and SXT/Yohkoh, *Astrophys. J.*, in press, 1998.

Lin, R. P., K. C. Hurley, D. M. Smith, R. M. Pelling, *Solar Phys., 135*, 57, 1991.

Mann, I., Dynamics of dust in the solar environment, in *Proc., First US–Russian Scientific Workshop on FIRE Environment*, IKI, Moscow, Russia, pp. 154–160, 1995 (JPL reorder no. 95-3).

Mann, I., and R. M. MacQueen, Ground-based observations of dust in the solar environment, in *Proc., First US–Russian Scientific Workshop on FIRE Environment*, IKI, Moscow, Russia, pp. 161–165,1995 (JPL reorder no. 95-3).

Marsch, E., MHD turbulence in the solar wind, in *Physics of the Inner Heliosphere*, R. Schwenn and E. Marsch, eds., Springer-Verlag, Berlin, p. 159, 1991.

Marsch, E., et al., Solar wind protons: Three-dimensional velocity distributions and derived plasma parameters measured between 0.3 and 1 AU, *J. Geophys. Res., 87*, 52–72, 1982.

McComas, D. J., et al., Structures in the polar solar wind: Plasma and field observations from Ulysses, *J. Geophys. Res., 100*, 19,893, 1995.

McComas, D. J., et al., Ulysses' return to the slow solar wind, *Geophys. Res. Lett., 25*, 1–4, 1998.

McNutt, R. L., Jr., et al., An ADvanced SOLar Probe Experiment Module (AD SOLEM), *SPIE Transactions* 2804, 2–13, 1996a.

McNutt, R. L., Jr., et al., A compact particle detector for low-energy particle measurements, *SPIE Transactions 2804*, 1996b.

Möbius, E., G. Gloeckler, B. Goldstein, S. Habbal, R. McNutt, J. Randolph, A. Title, and B. Tsurutani, Here comes Solar Probe! *Adv. Space Res.*, in press, 1999.

Moses, S. L., F. V. Coroniti, E. W. Greenstadt, and B. T. Tsurutani, Possible wave amplitudes in shocks in the solar corona: predictions for Solar Probe, *J. Geophys. Res., 96*, 21,397–21,401, 1991.

Murphy, G. B., D. R. Croley, M. Hoenk, S. Nikzad, R. W. Terhune, P. Grunthaner, and F. Grunthaner, CCD's as particle detectors—possibilities, problems and advances, in *Small Instruments for Space Physics, Proc. Small Inst. Workshop, Pasadena, CA,* B. T. Tsurutani, ed., NASA, Wash. D.C., pp. 4–15, 1993.

Neugebauer, M., L. A. Fisk, R. E. Gold, R. P. Lin, G. Newkirk, J. A. Simpson, and M. A. I. Van Hollebeke, *The Energetic Particle Environment of the Solar Probe Mission*, JPL 78–64, Jet Propulsion Laboratory, Pasadena, CA, 1978.

Neugebauer, M., et al., Ulysses observations of microstreams in the solar wind from coronal holes, *J. Geophys. Res., 100,* 23,389, 1995.

Okada, M., B. T. Tsurutani, B. E. Goldstein, A. L. Brinca, H. Matsumoto, and P. J. Kellogg, Investigation of possible electromagnetic disturbances caused by spacecraft plasma interaction at 4 R_S, in *Proc., First US–Russian Scientific Workshop on FIRE Environment*, IKI, Moscow, Russia, pp. 108–116, 1995 (JPL reorder no. 95-3).

Randolph, J. E., J. A. Ayon, K. Leschly, R. N. Miyake, B. T. Tsurutani, Innovations on the solar probe mission, *SPIE Transactions*, 1998.

Raymond, J., R. Suleiman, A. van Ballegooijen, and J. Kohl, Absolute abundances in streamers from UVCS, in *Correlated Phenomena at the Sun in the Heliosphere and in Geospace,* B. Fleck, ed., ESA SP-415, in press, 1998.

Reames, D. V., Particle acceleration in solar flares: Observations, in *Particle Acceleration in Cosmic Plasmas*, G. P. Zank and T. K. Gaisser, eds.**,** *AIP Conf. Proc. 264,* Newark, DE, p. 213, 1992.

Reames, D. V. Solar energetic particles: A paradigm shift, *Rev. Geophys. 33, Suppl.* (U. S. National Report to the IUGG, 1991–1994), p. 585, 1995.

Reames, D. V., Energetic particles and the structure of coronal mass ejections, in *Coronal Mass Ejections,* N. Crooker, J. A. Jocelyn, and J. Feynman, eds., *Geophys. Monogr. 99*, Amer. Geophys. Union, Washington, DC, p. 217, 1997

Reames, D. V., J. P. Meyer, and T. T. von Rosenvinge, Energetic-particle abundances in impulsive solar-flare events, *Astrophys. J. Suppl. Ser., 90*, 649, 1994.

Reames, D. V., L. M. Barbier, and C. K. Ng, The spatial distribution of particles accelerated by CME-driven shocks, *Astrophys. J. 466*, 473, 1996.

Schou, J., and the SOHO/SOI-MDI Internal Rotation Team, Helioseismic studies with SOI-MDI of differential rotation in the solar envelope, *Astrophys. J.*, Sept. 20, 1998.

Sheeley, N. R., et al., Measurements of flow speed in the corona between 2 and 30 R_S, *Astrophys. J., 484*, 472, 1997.

Skalsky, A. A., and V. E. Andreev, The dust in the solar system: the interplanetary space, the Jovian and Solar environments, in *Proc., First US–Russian Scientific Workshop on FIRE Environment*, IKI, Moscow, Russia, pp. 140–153,1995 (JPL reorder no. 95-3).

Suess, S. T., and E. J. Smith, Latitudinal dependence of the radial IMF component: Coronal imprint, *Geophys. Res. Lett., 23*, 3267, 1996.

Suess, S. T., et al., The geometric spreading of coronal plumes and coronal holes, *Sol. Phys., 180*, 213–246, 1998.

Tsintikidis, D., W. S. Kurth, D. A. Gurnett, and D. D. Barbosa, Study of dust in the vicinity of Dione using the Voyager 1 plasma wave instrument, *J. Geophys. Res., 100*, 1811–1822, 1995.

Tsurutani, B. T., and Lin, R. P, Acceleration of >47 keV Ions and >2 keV electrons by interplanetary shocks, *J. Geophys. Res*., 90, 1, 1985.

Tsurutani, B. T., and J. E. Randolph, *Origin and Evolution of Int. Dust,* A. Levaxeur-Regourd and H. Hasegawa, eds., Kluwer, p. 29, 1990.

Tsurutani, B. T., V. N. Oraevsky, H. Matsumoto, S. I. Klimov, et al., Report on Combined Atmospheric and Electromagnetic Environment Group, in *Proc., First US–Russian Scientific Workshop on FIRE Environment*, IKI, Moscow, Russia, pp. 256–258, 1995 (JPL reorder no. 95-3).

Tsurutani, B. T., K. Leschly, S. Nikzad et al., An integrated space physics instrument (ISPI) for Solar Probe, Am. Inst. Physics, CON970115, p. 131, 1997.

Vaisberg, O., and B. Tsurutani, eds., Solar Probe Environment Workshop, in *Proc., First*

US–Russian Scientific Workshop, Moscow, Russia, 1995 (JPL reorder no. 95-3).

Valentine, P. G., P. W. Trester, and R. O. Harrington, *Mass Loss Testing of Carbon–Carbon at High Temperatures*, General Atomic Report GA-C22515, 1997.

Wu, S. T., W. P. Guo, M. Dryer, B. T. Tsurutani, and O. L. Vaisberg, Evolution of Coronal MHD shocks into interplanetary MHD shocks, in *Proc.*, *First US–Russian Scientific Workshop on FIRE Environment*, IKI, Moscow, Russia, pp. 266–272, 1995 (JPL reorder no. 95-3).